12-9-2011

Kenaf bast for fiber reinforced polymer composites

Jinshu Shi

KENAF BAST FOR FIBER REINFORCED POLYMER COMPOSITES

By

Jinshu Shi

A Dissertation
Submitted to the Faculty of
Mississippi State University
in Partial Fulfillment of the Requirements
for the Degree of Doctor of Philosophy
in Forest Products
in the Department of Forest Products

Mississippi State, Mississippi

December 2011

KENAF BAST FOR FIBER REINFORCED POLYMER COMPOSITES

By

Jinshu Shi

Approved:

Sheldon Q. Shi Associate Professor of Forest Products (Director of Dissertation)	H. Michael Barnes Thompson Professor of Wood Science and Technology (Co-director of Dissertation)
Charles U. Pittman Professor of Chemistry (Committee Member)	Mark F. Horstemeyer Professor of Mechanical Engineering (Committee Member)
Giselle Thibaudeau Director of the Electron Microscope Center (Committee Member)	Rubin Shmulsky Professor of Forest Products (Graduate Coordinator of the Department of Forest products)
George M. Hopper (Dean of the College of Forest Resources)	

Name: Jinshu Shi

Date of Degree: December 9, 2011

Institution: Mississippi State University

Major Field: Forest Products

Major Professors: Sheldon Q. Shi and H. Michael Barnes

Title of Study: KENAF BAST FOR FIBER REINFORCED POLYMER COMPOSITES

Pages in Study: 86

Candidate for Degree of Doctor of Philosophy

Cellulosic fibers sized from the macro-scale to the nano-scale were prepared hierarchically from kenaf bast fibers using chemicals. The process began with a hermetical alkaline retting followed by a bleaching treatment. The bleached fibers were hydrolyzed using inorganic acid, from which microfibers and cellulose nanowhiskers (CNWs) were fabricated. Inorganic nanoparticle impregnation (INI) was used to treat the retted fibers for the improvement of the interfacial compatibility between the fiber and polypropylene (PP) matrix. The retted fibers and INI-treated fibers were used as reinforcement for the PP polymer composites. Film casting process was used to make CNW/PVA composites.

The hermetical retting process used in this study produced fibers with high cellulose contents (81-92%) by removing the lignin and hemicelluloses. Higher retting temperature resulted in higher fiber surface hardness and elastic moduli. The tensile strengths and tensile moduli of the fibers decreased as the temperature increased. The SEM images showed the micropores in the cell wall structure for the fibers retted at over 130 ℃, providing the possibility to anchor nanoparticles into the cell wall. Surface

morphology of the INI-treated fibers was examined with SEM, and showed that the $CaCO_3$ nanoparticle crystals grew onto the fiber surface. Energy-dispersive X-ray spectroscopy (EDS) was used to verify the $CaCO_3$ particle deposits on the fiber surface. As the size scale of the fibers decreased, the fiber crystallinity increased from 49.9% (retted fibers) to 83.9% (CNWs). About 23% α-cellulose in the raw kenaf bast fibers had been converted into CNWs.

The retted fibers without INI treatment had poor compatibility with the polypropylene matrix. The INI treatment improved the compatibility between the fibers and the PP matrix, resulting in an improvement in kenaf fiber/PP composite tensile moduli and tensile strengths. The CNWs prepared from kenaf bast fiber gave excellent reinforcement for PVA composites. A nine percent increase of CNWs in the CNW/PVA composites yielded significant improvements in tensile strength and modulus of about 46% and 152%, respectively, compared with pure PVA.

ACKNOWLEDGMENT

I would like to start by thanking my advisors, Prof. Sheldon Q. Shi and Prof. H. Michael Barnes.

I would like to thank my committee members, Prof. Mark Horstemeyer, Prof. Charles Pittman and Prof. Giselle Thibaudeau. A special thanks to Prof. Pittman for providing research advice.

I would like to acknowledge Dr. Sangyeob Lee, former Post-doctoral Research Associate in Forest Products Department, MSU, for training in instrumental operation and analysis. He also generously gave me constructive suggestions for my research methods and direction. Acknowledgements are given to Dr. Jinwu Wang, Dr. El Barbary M. Hassan, at Forest Product Department, MSU, to Mr. William A. Monroe and Ms. Amanda Lawrence, Research Associates in Electron Microscope Center (EM Center), MSU, and Mr. Stephen Horstemeyer, Laboratory Manager at CAVs, for their support and help. The International Center for Bamboo and Rattan (ICBR), Beijing, China, is acknowledged for instrumental support.

I would also like to thank the U.S. Department of Energy (DOE), funding # 362000-060803 through the Center for Advanced Vehicular System (CAVs) at Mississippi State University and National Science Foundation (NSF), fund # CMMI0928641 09080796 for their financial support of this research project.

TABLE OF CONTENTS

ACKNOWLEDGMENT ii

LIST OF TABLES vi

LIST OF FIGURES vii

CHAPTER

I. INTRODUCTION 1

1.1 Background 1
1.2 Literature review 2
1.2.1 Kenaf bast fibers 2
1.2.2 Application of kenaf bast fibers in polymer composites 3
1.2.3 Technical issues 5
1.2.4 Resolution of the technical issues 6
1.2.4.1 Alkaline retting 6
1.2.4.2 Inorganic nanoparticle impregnation technology 9
1.2.5 Cellulose nanowhisker (CNW) and its application in composites 10
1.2.5.1 Cellulose nanowhiskers (CNWs) 10
1.2.5.2 CNWs reinforced nanocomposites 13
1.3 Objectives 17

II. HERMETICAL ALKALINE RETTING TECHNOLOGY 18

2.1 Materials 18
2.2 Methods 18
2.2.1 Hermetical alkaline retting 18
2.2.2 Determination of the fibers yields and chemical components 19
2.2.3 Surface morphology analysis 19
2.2.4 Surface hardness and elastic modulus testing 20
2.2.5 Tensile properties testing 20
2.3 Results and discussion 21
2.3.1 Fiber yields and chemical components 21
2.3.2 Surface morphology analysis 23
2.3.3 Surface hardness and elastic moduli of the retted kenaf fibers 28

2.3.4 Tensile properties of the retted kenaf fibers 31
2.4 Conclusions 32

III. INORGANIC NANOPARTICLE IMPREGNATION TECHNOLOGY 33

3.1 Materials 33
3.2 Methods 33
3.2.1 Inorganic nanoparticle impregnation (INI) treatments 33
3.2.2 Determination of $CaCO_3$ loading weight percentages 35
3.2.3 Surface morphology and elemental analysis 36
3.2.4 Surface hardness and elastic modulus testing 37
3.3 Results and discussion 37
3.3.1 $CaCO_3$ loading weight percentages 37
3.3.2 Surface morphology and elemental analysis 38
3.3.3 Surface hardness and elastic moduli of the INI-treated kenaf fibers 41
3.4 Conclusions 43

IV. PREPARATION OF CELLULOSE NANOWHISKERS 44

4.1 Materials 44
4.2 Methods 44
4.2.1 Preparation of CNWs 44
4.2.2 Determination of fiber yields and chemical components 45
4.2.3 Surface morphology analysis 46
4.2.4 Functional group analysis 46
4.2.5 Determination of the fiber crystallinity 47
4.3 Results and discussion 47
4.3.1 Hierarchical yields and chemical components 47
4.3.2 Surface morphology analysis 50
4.3.3 Fiber dimension analysis 52
4.3.4 Fourier Transform Infrared spectroscopy 53
4.3.5 Fiber crystallinity 54
4.4 Conclusions 56

V. POLYMER COMPOSITES REINFORCED WITH KENAF BAST FIBERS 57

5.1 Materials 57
5.2 Methods 57
5.2.1 Fabrication of kenaf fiber/PP composites 57
5.2.2 Fabrication of CNW/PVA composites 58
5.2.3 Dimensional analysis of CNWs 59
5.2.4 Composites tensile properties testing 59
5.2.5 Thermal properties analysis 60
5.3 Results and discussion 61

5.3.1 Kenaf fiber/PP composites 61
5.3.1.1 Tensile properties of the retted kenaf fiber/PP composites 61
5.3.1.2 Tensile properties of the INI-treated kenaf fiber/PP composites 64
5.3.1.3 Thermal properties of the kenaf fiber/PP composites.....67
5.3.2 CNW/PVA composites.....69
5.3.2.1 Distributions of CNWs dimensions in CNW/PVA composites.....69
5.3.2.2 Tensile properties of CNW/PVA composites.....71
5.4 Conclusions 75

VI. SUMMARY AND FUTURE WORK 76

6.1 Summary 76
6.2 Future work 77

REFERENCES 78

LIST OF TABLES

2.1 Average and standard deviation of the fiber dimensions.....24

3.1 Six reaction conditions for INI treatments.....35

4.1 Dimensions of the hierarchical fibers 52

5.1 Thermal characteristics of the kenaf fiber/PP composites and pure PP.....68

5.2 Lengths and diameters of CNWs in the CNW/PVA composite 70

LIST OF FIGURES

2.1 Yields and chemical components of the retted kenaf fibers 21

2.2 Images of the retted kenaf fibers. The labels mean the retting temperatures. 23

2.3 Length distributions of the retted kenaf fibers 25

2.4 Diameter distributions of the retted kenaf fibers 25

2.5 Aspect ratio distributions of the retted kenaf fibers 26

2.6 SEM images of the cell wall of the retted kenaf fibers. The labels mean the retting temperatures. Arrows designate the micropores 27

2.7 Surface hardness of the retted kenaf fibers. The labels mean the retting temperatures 28

2.8 Elastic moduli of the retted kenaf fibers. The labels mean the retting temperatures 28

2.9 Tensile properties of the individual retted kenaf fibers. The labels mean the retting temperatures. 31

3.1 Flowchart of the INI treatments 34

3.2 Weight percentages of $CaCO_3$ loading of INI-treated kenaf fibers. The labels mean the molar ratios of Na_2CO_3 to $CaCl_2$ and the reaction temperatures 37

3.3 SEM images of INI-treated kenaf fibers. 1:1 and 1:2 means the molar ratios of Na_2CO_3 to $CaCl_2$. The temperatures mean the reaction temperatures. The arrows designate $CaCO_3$ particles. 38

3.4 EDS spectrum of the control fiber 40

3.5 EDS spectrum of INI-treated kenaf fiber 40

3.6 Surface hardness of the INI-treated kenaf fibers. The labels mean the molar ratios of Na_2CO_3 to $CaCl_2$ and the reaction temperatures.....41

3.7 Elastic moduli of the INI-treated kenaf fibers. The labels mean the molar ratios of Na_2CO_3 to $CaCl_2$ and the reaction temperatures.....41

4.1 Yields and chemical components of the hierarchical fibers.....48

4.2 SEM images of kenaf bast, retted fiber, bleached fiber and microfiber.....50

4.3 TEM images of CNWs. The labels mean the magnifications.....51

4.4 FT-IR spectra of the hierarchical fibers.....54

4.5 X-ray diffraction spectra of the hierarchical fibers.....55

4.6 Crystallinities of the hierarchical fibers.....55

5.1 Tensile strength of retted kenaf fiber/PP composites.....61

5.2 Tensile moduli of the retted kenaf fiber/PP composites.....62

5.3 Stress-strain curves of the retted kenaf fiber/PP composites.....62

5.4 Fracture surface SEM images of the retted kenaf fiber/PP composites. The kenaf fibers were retted at (a) 80 ℃, (b) 110 ℃, (c) 130 ℃ and (d) 160 ℃.....63

5.5 Tensile strengths of INI-treated kenaf fiber/PP composites. The labels mean the INI treatments conditions for the kenaf fibers. Non-INI treated fiber is the fibers retted at 160°C but not treated with INI processes.....64

5.6 Tensile moduli of INI-treated kenaf Fiber/PP composites. The labels mean the INI treatments conditions for the kenaf fibers. Non-INI treated fiber is the fibers retted at 160°C but not treated with INI processes.....64

5.7 Stress-strain curves of the INI-treated fiber/PP composites. The labels mean the INI treatments conditions for the kenaf fibers. Non-INI treated fiber is the fibers retted at 160°C but not treated with INI processes.....65

5.8 SEM images of the fractural surfaces of INI-treated kenaf fiber/PP composites. The labels mean the reaction temperatures and the molar ratios of Na_2CO_3 to $CaCl_2$. Non-INI treated fiber is the fibers retted at 160°C but not treated with INI processes.....67

5.9 TEM images of CNW/PVA composites. Magnification = 14,000X.
(a) Weight ratio of CNW=1%; (b) Weight ratio of CNW=3%;
(c) Weight ratio of CNW=6%; (d) Weight ratio of CNW=9%.....70

5.10 Length and diameter distributions of CNWs before and after incorporation in the CNW/PVA composite. The CNW/PVA composite contains 9 % CNWs.....70

5.11 Tensile strengths of the CNW/PVA composites.....71

5.12 Tensile moduli of the CNW/PVA composites.....72

5.13 Stree-strain curves of the CNW/PVA composites.....73

5.14 SEM Images of fracture surfaces of CNW/PVA composites.
(a) pure PVA; (b) CNW/PVA composites with 3% CNWs;
(c) CNW/PVA composites with 9% CNWs 74

CHAPTER I

INTRODUCTION

1.1 Background

Two types of fibers are commonly used as reinforcements in polymer composites: synthetic fibers such as glass or carbon fibers, and natural fibers including kenaf, flax, hemp, sisal, etc. Although the glass fiber reinforced plastic composites meet structural and durability demands, they have shortcomings—their relatively high fiber density, difficulty to machine, poor recycling properties, and the potential health hazards posed by glass fiber particulates (Holbery and Houston 2006).

Natural fibers are environmentally friendly and sustainable materials, which can be used to replace synthetic fibers in composite industry. Natural fibers have advantages over synthetic fibers including low cost, low density, comparable specific strength properties, ease of separation, ease of recycle, decreased energy of fabrication, and CO_2 neutrality (Mohanty 2000). For instance, the energy consumption to produce a flax fiber mat is approximately 9.55 MJ/Kg from cultivation and harvesting to fiber separation, compared to 54.7 MJ/kg to produce a glass fiber mat. Thus, producing a flax fiber mat saves 17% of the production energy (Joshi *et al*. 2004).

The term “natural fibers” covers a broad range of vegetable, animal, and mineral fibers. In the composites industry this term usually refers to wood fiber and

agro-based fibers. Natural fibers can be derived from the bast, leaf, seed, and stem of plants. The most popular natural fibers used in the composites include the bast fibers of kenaf, hemp, and sisal leaf fibers.

Wambua *et al*. (2003) fabricated and tested polypropylene composites using different natural fibers as reinforcements, including 40% fiber content of kenaf, coir, sisal, hemp, and jute respectively. The mechanical properties of the natural fiber composites were comparable with those of the glass mat polypropylene composites. In some cases, the specific properties of the natural fiber composites were better than those of glass fiber composites, suggesting the natural fiber composites have a potential to replace glass in some applications. Mohanty *et al*. (2002) reported the density of natural fibers such as kenaf, jute, hemp, flax, and sisal were much lower than that of the traditional reinforcement materials, and the strength/weight ratios were comparable to widely used materials, such as E-glass and Aramid.

1.2 Literature review

1.2.1 Kenaf bast fibers

Kenaf (*Hibiscus cannabinus)* is an agricultural crop whose history of cultivation can be traced back to ancient Africa. Kenaf grows quickly, rising to 12 to 14 feet in 4 to 5 months. In the United States, kenaf is cultivated in many states, including Mississippi, Texas, and California. Kenaf yields 6 to 8 metric tons of bast and core per acre annually (Kaldor *et al*. 1990). The advantages of kenaf fibers over other conventional fiber crops like jute, hemp, and flax include short growing time, easy adaptability to climatic

conditions, and relatively low use of herbicides and pesticides (Wang and Ramaswamy 2003).

The major components of kenaf bast fiber are cellulose, hemicellulose, lignin, and pectin (Mwaikambo 2006). Due to the relatively high cellulosic contents, kenaf fibers are used as a source of paper, grass mats, oil-absorbent materials, animal bedding, and textiles (Lloyd and Seber 2006; Keshk *et al*. 2006). The environmentally friendly properties of kenaf include the following factors: (a) kenaf accumulates carbon dioxide at a significantly high rate (Zampaloni *et al*. 2007); (b) kenaf absorbs nitrogen and phosphorous from the soil (Michell 1986); (c) it is easily recycled (Mohanty 2000); and (d) kenaf fiber's light weight composites improve fuel efficiency and reduce emissions, especially in automotive applications (Joshi *et al*. 2004). Commercially grown in the United States, kenaf maintains a competitive price of approximately $0.44–$0.55/kg, compared to $2.00–$3.25/kg for E-glass (Mohanty 2000). In the European automotive industry, the consumption of kenaf fibers increased from 1,100 tons in 1999 to 2,000 tons in 2000 (Bledzki *et al*. 2002).

1.2.2 Application of kenaf bast fibers in polymer composites

Sanadi *et al*. (2001) fabricated high kenaf fiber content polypropylene (PP) composites (kenaf fiber: PP= 85:15 by weight) with a superior flexural modulus and strength compared to many formaldehyde-based low and medium density fiber boards. Clemons and Sanadi (2007) conducted instrumented Izod tests on the kenaf fiber reinforced PP composites, and showed that with a coupling agent the incorporation of kenaf fibers improved composites impact property. The energy to maximum load (EML) values for the kenaf composites in reversed notch impact tests were about half of those

unfilled PP specimens at +25 ℃, but slightly higher at -25 ℃ than unfilled PP specimens. Kenaf fibers offer significant benefits in impact performance over wood powder, at both low (-50 ℃) and high (+50 ℃) temperatures. Takashi *et al*. (2003) fabricated kenaf fiber/poly-l-lactic acid (PLLA) composites with a fiber content of 70%. The Young's modulus and tensile strength were 6.3 GPa and 62 MPa respectively. These properties were higher than those of pure PLLA film. Shibata *et al*. (2006) made laminate composites from kenaf and PP fibers. The flexural modulus increased with the increase of the number of kenaf layers and heating time. An increase of the number of kenaf layers contributed to homogeneous PP dispersion in the composite board. The increased heating time contributed to a better wetting between kenaf and PP. Aziz *et al*. (2005) prepared kenaf fiber reinforced-unsaturated polyester composites. The kenaf fibers were alkalized with 6% NaOH solution before being incorporated with polyester. The unsaturated polyester resin was modified to be more polar to increase compatibility with kenaf fiber surfaces. The modification resulted in a significant improvement in the composites flexural strengths and flexural moduli. Lee *et al*. (2010) fabricated PP composites both unidirectionally and randomly reinforced with bacterial-retted kenaf bast fibers. The uniaxial fiber orientation improved the composites flexural and tensile properties along the fiber axial direction. The randomly oriented kenaf fibers provided an equal performance to the composites made of 25% fiber glass reinforced polyvinyl ester resin.

1.2.3 Technical issues

Homogenization of the fiber's distribution, adhesion between the fiber and matrix, moisture and flame retardant properties can be technical issues for the kenaf based composites (Holbery and Houston 2006).

Zampaloni *et al*. (2007) indicated kenaf fibers were poorly dispersed during manufacturing. Three methods were used to fabricate kenaf fiber-reinforced PP composites. In the first method, PP sheets were prepared, followed by sandwiching kenaf fibers (long fibers, approximately 130 mm, and shorter fibers, approximately 20 mm) between two layers of PP sheets. The samples showed extremely poor fiber distribution. In the second method, the chopped kenaf fibers were mechanically mixed with PP powders with a kitchen mixer. With this method, the mixer balled up the kenaf and the denser PP fell through to the bottom of the mixer. The powder had to be spread more evenly though the fibers by hand mixing. However, there was a tendency for the fibers to create a swirling pattern, causing clumping and voids, which made it difficult to achieve an even fiber distribution. In the third method, a sifting process was employed, involving sprinkling the PP powder as a base layer, adding individually sifted fibers, sprinkling more PP, etc. until all the desired materials were used. A better fiber distribution was achieved by this method when a 34.8 mm square sample was made. However, it was not suitable for fabricating larger samples.

The role of the matrix in a fiber reinforced composite is to transfer the stress to the reinforcing fibers through shear stresses at the interface. It is essential to obtain a good interfacial bonding between the polymeric matrix and the fibers. Poor compatibility between hydrophobic polymers and hydrophilic fibers would result in poor mechanical

properties of the composites. The effect of chemically treating coir, banana, and sisal fibers with sodium alginate and sodium hydroxide has been reported by Mani *et al*. (1990). The modification resulted in an increase in adhesive bonding and thus improved the ultimate tensile strength up to 30%.

Alkali treatment, dinitrophenylation, benzoylation, and benzoylation-acetylation were carried out on pineapple leaf fibers by Samal and Ray (1997). Except for the benzoylated fibers, the other fibers yielded an improvement in their mechanical strength. The mechanical strength of the alkali treated fiber yielded a 66.7% increase compared to the untreated fibers. Kuruvilla *et al*. (1996) investigated the influence of chemically treating sisal fiber with sodium hydroxide, isocyanate, and peroxide on the properties of sisal/polyethylene composites. These treatments increased the tensile strengths and moduli of the composites compared to those reinforced with the untreated fibers.

1.2.4 Resolution of the technical issues

1.2.4.1 Alkaline retting

Alkaline retting treatment can remove lignin and hemicellulose from kenaf bast fibers and liberate individual cellulosic fibers from the larger fiber bundles. The resultant fibers have relatively homogeneous dimensions, and are easily suspended in water. Fiber sheets in which the fibers are distributed uniformly can then be made by a method similar to the paper-making process. A sheet molding compound (SMC) process can be applied to fabricate composites with alternatively laminated fiber/polymer mats. The molten polymer penetrates the fiber sheets during hot pressing. When the mat is cooled, the

polymer crystallizes and the fibers combine with the polymer matrix with a uniform distribution.

Similar to many other natural fibers, kenaf fiber is composed of cellulose, hemicellulose, and lignin. Cellulose is the major framework component of the fiber. It is a highly crystalline, linear polymer of anhydroglucose molecules, with a degree of polymerization of around 10,000. Cellulose is the main component providing strength, stiffness, and structural stability (Clemons 2005). Hemicelluloses are branched polymers containing five-and six-carbon sugars of varied chemical structure. The molecular weights of hemicellulose are much smaller than those of cellulose. Lignin is an amorphous, cross-linked polymer network, consisting of an irregular array of variously bonded hydroxy-and methoxy-substituted phenylpropane units (Pettersen 1984).

Fiber retting is conducted for kenaf bast to remove the hemicelluloses and lignin. Several different retting methods are used (Holbery and Houston 2006). These include: (1) Dew retting is conducted in the field when the stalk is harvested. Rain, dew, or irrigation is used to keep the stems moist. This method may take up to five weeks and produces a coarse fiber with a light brown color; (2) Water retting is conducted in water. Aqueous bacteria break down the pectin. This takes seven to ten days and produces quality fibers; (3) Warm-water retting begins with water immersion of the batch for twenty-four hours, followed by warming up the batch for two or three days. This method produces uniform and clean fibers; (4) Mechanical processing is usually used to prepare fibers for textiles, paper, or fiberboard products application; and (5) Chemical retting uses chemicals to dissolve the pectin and separate the components. This is a quick process and produces high quality fibers.

Alkaline retting rapidly removes nonfibrous materials, including lignin and hemicellulose, causing fiber swelling and separation. The remnant lignin and hemicellulose contents of the retted fibers vary with the concentration of alkali agent. The higher the alkali agent concentration, the lower the lignin and hemicellulose contents became (Lee *et al*. 2003).

Song and Obendorf (2006) retted kenaf fiber with NaOH, bacteria, and enzyme respectively. The syringyl lignin content was reduced by all of the methods. Parikh *et al*. (2002) developed an improved chemical retting process using a special caustic formulation for effective retting, and a special soap finish for improved carding of kenaf fibers. The resultant fibers were not suitable for automotive applications, although they showed good luster, strength, and flexibility. Morrison *et al*. (1996) retted kenaf fibers in boiling 7% NaOH and 0.5% $NaHSO_4$ for one hour. Gas-liquid chromatographic analysis and ultraviolet absorption microspectrophotometry indicated the lignin and hemicellulose contents were both degraded and the amount was reduced after retting, while the cellulose content did not decrease. Ramaswamy *et al*. (1994) retted kenaf fibers using both bacterial and chemical methods. The bacterial method lasted for ten days. The chemical method employed 7% NaOH at its boiling point for 1 hr. The residual gum contents (lignin, waxes, hemicellulose, and pentosans) of the bacterially retted fibers and chemically retted fibers were 21-23% and 7-12% respectively. The non-cellulosic components content in the fibers was still high, and the fibers were still not easily distributed uniformly in polymer composites. Salam *et al*. (2007) delignified and bleached kenaf fibers using sodium sulfite, monoethanolamine, and soda ash. The delignification treatment removed 40-45% of the lignin from the raw kenaf fibers.

Although this research demonstrated that alkaline retting treatment could effectively prepare cellulosic fibers by removing lignin and hemicellulose, the removal of these components was not complete. The fibers can be separated into much smaller and more homogeneous dimensions by completing the decomposition of hemicellulose and lignin in alkaline solution. As the cellulose content of the retted fibers increases, the distribution of these fibers in composites is more uniform.

1.2.4.2 Inorganic nanoparticle impregnation technology

Micropores were generated by alkaline retting because of the removal of lignin and hemicellulose (Allan *et al*. 1992). The porous structure of the fibers causes air bubbles in composites and results in defects in the final products. The air bubbles cannot transfer stress when the material is under load and yield fracture initiation at the bubble-matrix interface. One way to eliminate the defects is to fill the micropores.

Inorganic mineral fillers such as calcium carbonate ($CaCO_3$), clay, TiO_2, and talc have been widely used in pulp and paper industries. The purpose of these fillers is to reduce the cost of paper and to improve the brightness, opacity and the printability of the paper (Othman *et al*. 2010). $CaCO_3$ is the most popular material applied as a filler in paper industry because of its low cost and ease of fabrication. Two types of $CaCO_3$ are usually employed. One is ground calcium carbonate (GCC) which is made from natural calcium carbonates. The other is precipitated calcium carbonate (PCC) which is synthetic calcium carbonate produced by a recarbonisation process (IMA-Europe 2006). $CaCO_3$ nanoparticles can be synthesized by reacting calcium chloride ($CaCl_2$) with sodium carbonate (Na_2CO_3). The aqueous solutions of these salts, as precursors, penetrate easily

into the porous structures of kenaf fibers. $CaCO_3$ precipitation can be generated in the micropores where the precursors are loaded. The reaction is described below.

$$CaCl_2 \cdot H_2O + Na_2CO_3 \xrightarrow{H_2O} CaCO_3 + 2NaCl + 2H_2O \quad (1.1)$$

The $CaCO_3$ nanoparticles not only fill up the micropores in the cell wall of the retted fibers, but also work as nucleation sites for polymer matrix in the composites. Lee *et al*. (2007) indicated that the nanoparticles deposited on natural fiber surfaces may serve as heterogeneous nucleation sites to initiate the crystalline orientation of the molten polymer matrix. Lee (2007) applied inorganic nanoparticle impregnation (INI) technology to treat wood fibers. The INI technology included consecutive impregnation of Na_2CO_3 and $CaCl_2$ aqueous solutions in wood fibers. The $CaCO_3$ particles were synthesized in the fiber cell wall. The effects of reaction time, temperature, and ionic salt ratios on the size of $CaCO_3$ crystals were evaluated.

1.2.5 Cellulose nanowhisker (CNW) and its application in composites

1.2.5.1 Cellulose nanowhiskers (CNWs)

Cellulose plays the most important role in providing mechanical support for natural fibers. Cellulose, an organic compound with the formula $(C_6H_{10}O_5)_n$, is a polysaccharide consisting of a linear chain of several hundred to over ten thousand β(1-4) linked D-glucose units (Updegraff 1969). Up to 100 glucon chains are grouped together to form long thin crystallites which are called elementary fibrils. These crystallites are about 5 nm wide, varying with the source of the cellulose (Alemdar and Sain 2008). They are organized in groups to form microfibrils 8-50 nm in diameter and a few microns

in length (Clowes and Juniper 1968). The crystalline regions represent a tight packing of ordered chains, where the cellulose molecule chains are bonded by hydrogen bonding. The crystalline regions are difficult to penetrate with chemical reagents. Cellulose also contains less ordered amorphous regions. Since interchain bonding is minimal in the amorphous regions, chemical reagents can more easily diffuse or penetrate in these regions (Lewin 2006). Cellulose fibers can either be man-made (cellulose II) or natural (cellulose I). The crystal structures of the native and regenerated celluloses are known as cellulose I and II respectively (Eichhorn *et al*. 2001). The chains within the unit cell are in parallel conformation in cellulose I, and in antiparallel conformation in cellulose II (Woodcock and Sarko 1980; Sarko and Muggli 1974).

Zadorecki and Michell (1989) reported the elastic moduli of solid wood, single pulp fiber, microfibrils, and crystallites were 10 GPa, 40 GPa, 70 GPa and 250 GPa respectively. Additional studies were carried out to evaluate the elastic modulus of the crystalline regions. The elastic modulus (E) of the crystalline regions of cellulose polymorphs in the direction parallel to the chain axis was measured by x-ray diffraction (Nishino *et al.* 1995). The E values of cellulose I, II, III_I, III_{II}, and IV_I were 138, 88, 87, 58, and 75 GPa respectively. Rusli and Eichhorn (2008) determined the stiffness of CNWs using Raman spectroscopy. Their report showed the stiffness of a single CNW was between 105 GPa for a 3 dimensional network of the fibers, and 57 GPa for a 2 dimensional in-plane random orientation of the fibers. The propagation energy loss in the cellulosic materials during the stress loading was ignored in Sturcova's study (2005). Consequently, the values of elastic modulus for cellulose crystals obtained by Sturcova should be slightly larger than the true values. The data indicates the hierarchical

defibrillation of natural fibers from macro to micro to nano scale will produce cellulosic fibers with higher crystallinity.

Cellulose nanofibers have been prepared from different sources including cotton linter (Roohani *et al*. 2008), flax bast fiber (Bhatnagar and Sain 2005; Qua *et al*. 2009), hemp fiber (Bhatnagar and Sain 2005), kraft pulp (Bhatnagar and Sain 2005; Lu *et al*. 2008), rutabaga (Bhatnagar and Sain 2005), and microcrystalline cellulose (Lee *et al*. 2009). Technologies to prepare cellulose nanofibers have been reported, including an enzymic method (Henriksson *et al*. 2007), a bacterial method (Tsuchida and Yoshinaga 1997), cryocrushing (Chakraborty *et al*. 2005), a grinding treatment (Iwamoto *et al*. 2005), and an ultrasonic technique (Wang *et al*. 2006). All these methods require using a combination of chemical, mechanical, and other processes to prepare cellulose nanofibers from raw natural fibers. The resultant cellulose nanofibers had different morphologies, such as entangled network or rod-like nanoparticles. Different terminologies have been used to designate the rod-like nanofibers—nanowhiskers, monocrystals, nanocrystals, etc. (Siqueira *et al*. 2009). In this study, we use the term cellulose nanowhisker (CNW).

Bleached and unbleached kenaf fibers were used to prepare nanofibers (Jonoobi *et al*. 2009) using a combination of chemical and mechanical treatments. The chemical methods were based on NaOH-AQ (anthraquinone) and a three-stage bleaching process, whereas the mechanical techniques involve refining, cryocrushing, and high pressure homogenization. The resultant fiber had diameters between 10 nm and 90 nm. The crystallinity of the nanofibers prepared from unbleached fibers and bleached fibers increased to 79.2% and 81.4% respectively from 48.2%, the value for the raw kenaf fibers. However, the SEM images showed the nanofibers twisted and formed into a non-

uniform network. This result indicated fiber distribution difficulties in polymer composites.

1.2.5.2 CNWs reinforced nanocomposites

Different types of nano or micro cellulosic fibers have been applied as reinforcements in polymer nanocomposites. These polymer nanocomposites showed high strength, low thermal expansion, high thermal stability, thermal conductivity, and optical transparency (Berglund and Peijs 2010). Due to the heterogeneous structure and composition of natural fibers, and insufficient fiber-matrix compatibility, typical random-oriented natural fiber-reinforced composites showed a tensile strength of 15-140 MPa and an elastic modulus of 1-13 GPa (Gindl and Keckes 2005). Cellulose fiber-reinforced phenol-formaldehyde composites with bending strength of 370 MPa were produced using cellulose nanofibrils obtained by the microfibrillation of wood pulp (Nakagaito and Yano 2005).

An important factor to take into consideration is how to combine micro- and nano-fibers with a polymer matrix. The micro- and nano-fibers can be easily suspended in water, but many polymers used in composites are insoluble in water. Organic solvents which can swell micro- or nano-fibers, such as dimethylformamide (DMF), are usually combined with a nonpolar polymer matrix such as polyurethane. Otherwise, the microfibers or nanofibers are directly suspended in water soluble polymers such as starch and polyvinyl alcohol (PVA).

A high strength elastomeric nanocomposite was successfully prepared by dispersing microcrystalline cellulose in a polyurethane matrix using DMF as a medium (Wu *et al*. 2007). The nanocomposites yielded an improvement in strain-to-failure and

increased stiffness and strength compared to the unfilled polyurethane. The average tensile strength for this composite was 257 MPa, compared with 39 MPa for the neat polyurethane. The Young's Modulus of the composite was 12.9 MPa, higher than that of neat polyureathane.

DMF was used as a medium to fabricate polyurethane composites reinforced with nano- and micron-sized cellulose crystals (Marcovich *et al*. 2006). A strong filler-matrix interaction was developed during curing as a result of a chemical reaction between the crystals and the isocyanate component.

Iwatake *et al*. (2008) prepared poly (lactic acid) (PLA) composites reinforced with microfibrillated cellulose (MFC) using acetone. PLA was dissolved in an acetone suspension of MFC (1 wt %). Composites were formed by the evaporation of acetone when the mixture was kneaded. The MFC increased the Young's modulus and tensile strength of PLA by 40% and 25% respectively, without a reduction of yield strain at a fiber content of 10 wt%. Needle-leaf bleached kraft pulp reduced the yield strain by 30% and reduced the strength by 15% at a fiber content of 5 wt%.

A compounding extrusion process was used by Oksman (2006). He prepared PLA composites reinforced with cellulose whiskers prepared from commercial microcrystalline cellulose (MCC). MCC was treated with N,N-dimethylacetamide (DMAc) containing lithium chloride (LiCl) to swell the MCC and partly separate the cellulose whiskers. The suspension of whiskers was pumped into the polymer melt during the extrusion process. The research demonstrated that DMAc/LiCl can be used as a swelling or separation agent for MCC, but seems to cause degradation of the composites at high temperature processing.

Gindl and Keckes (2005) prepared cellulose-based nanocomposites films with microcrystalline cellulose powder partially dissolved in lithium chloride/DMAc by a film casting process. The composites films were isotropic, transparent to visible light, and highly crystalline. The mechanical properties of the composites depended on the composition ratio. The tensile strengths up to 240 MPa were observed, and the elastic moduli values were as high as 13.1 GPa.

Another method to produce cellulose nanofiber/nonpolar polymer composites was an organic solvent exchange method. In Nogi's study (2006), the initial suspension medium of bacterial cellulose was water. It was replaced with acetone gradually. Then, the cellulose was impregnated with neat acrylic resin. Nanocomposites with lower fiber contents in a range of 19.0-49.0 wt % were formed by UV curing. The composites made of cellulose nanofibers and acrylic resin were also prepared by the impregnation of the nanofibers mat with acrylic resin followed by UV curing of the resin (Iwamoto *et al*. 2005; Nogi *et al*. 2005). The composites demonstrated good optical transparency.

Alemdar and Sain (2008) used cellulose nanofibers obtained from agro-residues to reinforce thermoplastic starch. No organic solvent was applied because the nanofibers and starch matrix were both hydrophilic. In the study, the nanofibers were distributed uniformly in starch. The tensile strength and modulus of the nanocomposite films increased significantly compared to the pure thermoplastic starch. Dynamic mechanical analysis values of the storage modulus increased from 112 MPa for the pure thermoplastic starch to 308 MPa for the thermoplastic starch composites reinforced with 10 wt% nanofibers. Glass transition temperature increased with nanofibers loading.

Another water soluble polymer used to fabricate nanofiber reinforced composites is poly(vinyl alcohol) (PVA). The water suspension of cellulose nanowhiskers can be mixed with PVA water solution directly. A composite is formed through the evaporation of water. This process is called the "solution casting" or "film casting" technique. Tang and Liu (2008) reported the fabrication and characterization of PVA composite film reinforced with high volumes of electrospun cellulose nanofibrous mat (CNM). The composite film reinforced with 40 wt% CNM exhibited visible light transmittance of 75%. The mechanical strength and the Young's modulus were increased by 50% and 600% respectively, compared to neat PVA films.

The solution casting process was applied by many other researchers to prepare PVA composites reinforced with cellulose nanofibers (Leitner *et al*. 2007), microcrystalline cellulose (Lee *et al*. 2009), or microfibrillated cellulose (Lu *et al*. 2008; Qua 2009). This research demonstrated that different types of cellulose nanofibers enhanced the tensile strength and Young's modulus of the PVA composites.

A report by Bhatnagar and Sain (2005) indicated the cellulose nanofibers prepared from different resources, such as hemp, rutabaga, flax, and kraft pulp, would present different reinforcement effects for PVA. Kvien and Oksman (2007) achieved the alignment of CNWs in PVA composites with a strong magnetic field (7T). With 2 wt % CNWs incorporated in a PVA matrix, the CNWs were oriented perpendicular to the direction of the magnetic field. The dynamic modulus of the nanocomposite was around 2 GPa higher at room temperature in the aligned direction than in the transverse direction.

In a report by Roohani *et al*. (2008), nanocomposites were also prepared from copolymers of PVA/polyvinyl acetate (PVAc) and a colloidal aqueous suspension of

CNWs. These results showed stronger filler/matrix interaction existed in fully hydrolyzed PVA, compared to partially hydrolyzed samples. In this study, the CNWs prepared from kenaf bast using an all chemical process will be applied to reinforce PVA composites. The CNW will be characterized and its reinforcement effects on PVA composites will be investigated.

1.3 Objectives

The objectives of this study are: (1) to prepare individual cellulosic fibers by alkaline retting treatment from kenaf bast fiber; (2) to evaluate the effects of INI treatments on the characteristics of the kenaf fibers and on the properties of the PP composites reinforced with the fibers; (3) to prepare CNWs from kenaf bast using an all-chemical process; and (4) to investigate the reinforcement effects of CNWs on PVA composites.

CHAPTER II

HERMETICAL ALKALINE RETTING TECHNOLOGY

2.1 Materials

Kenaf bast was harvested from the Mississippi State University (MSU) North Farm in January 2007. The bast was cut into 50.8 mm lengths. The moisture content was 8.1% before the retting process was applied. Sodium hydroxide (NaOH) aqueous solution (5%) was prepared with distilled water and NaOH beads (Lab grade, Thermo Fisher Scientific Inc.). Acetic acid (17.4N, Reagent grade, Thermo Fisher Scientific Inc.) was used to adjust pH of the retting liquid.

2.2 Methods

2.2.1 Hermetical alkaline retting

Kenaf bast was retted with a 5% NaOH solution (fiber: NaOH solution = 1: 30, g: ml) in a hermetical reactor (Parr Instrument Co. 251M) at four temperatures (80 ℃, 110 ℃, 130 ℃ and 160 ℃). The retting process took one hour and was aided with a mechanical stirring. The autogeneous vapor pressures were 0.05 MPa at 80 ℃, 0.15 MPa at 110 ℃, 0.27 MPa at 130 ℃, and 0.60 MPa at 160 ℃. After the retting process, the pH of the retting liquid and retted fibers was adjusted to 7.0 using acetic acid. The neutralized fibers were washed with water to remove chemicals. The retted fibers were oven dried at

103℃, or freeze-dried, until moisture was completely removed. Freeze-dried, moisture-free fibers were used for the determination of chemical components, morphology, tensile testing, and nanoindentation testing. The oven-dried moisture-free fibers were used for inorganic nanoparticle impregnation (INI) treatments and composite fabrication.

2.2.2 Determination of the fibers yields and chemical components

Chemical components including hollocellulose, α-cellulose, Klason lignin, and ash content were determined for both the raw kenaf bast and the retted fibers. The ash content was measured using the TAPPI standard T 211-om 93 (TAPPI 1993). The determination of Klason lignin was based on the constituent insoluble in 72% sulfuric acid, which was estimated in accordance with method No. 482 of the Institute of Paper Chemistry (1951). Hollocellulose, the total polysaccharide fraction (cellulose and hemicelluloses) of the fibers, was estimated according to the method used by Wise *et al*. (1946). α-Cellulose is the part of cellulose which does not dissolve in 17.5% sodium hydroxide solution, and was determined in accordance to the method from the German Association of Cellulose Chemists and Engineers (1951). The yields of retted fibers were obtained based on the ratio of the oven-dried weights of the resultant fibers to the original weights of the raw kenaf bast

2.2.3 Surface morphology analysis

A Zeiss SupraTM 40-Gemini® Scanning Electron Microscope (SEM) was used to study the morphology of the retted fibers with an accelerating voltage of 15 kV. The fibers were coated with gold sputtering to give a 15 nm thick before being scanned. Seventy individual retted fibers (160°C) and mechanically disintegrated fibers were

randomly selected and images were acquired with the SEM. Fibers dimensions were measured, and the distributions of their lengths, diameters and aspect ratios were statistically studied.

2.2.4 Surface hardness and elastic modulus testing

A Hysitron TriboIndenter with a Berkovich diamond tip was used to test the fibers' surface hardness and elastic moduli at a 400 μN peak force and a 40 μN/s loading rate using a 10 second segment time. The fibers were mounted in a hardened epoxy matrix, and the load was perpendicular to the longitudinal direction of the fibers. According to the elastic punch theory and Oliver and Pharr's method (1992), the reduced elastic moduli can be obtained based on the elastic contact stiffness.

2.2.5 Tensile properties testing

The tensile properties of the individual retted fibers were investigated at the International Center for bamboo and Rattan (ICBR), Beijing, China, using a newly developed microtester (SF-I) (Wang *et al*. 2011). Thirty individual fibers retted at 110 ℃ and 160 ℃ were tested respectively. The nominal gauge length was 0.7 mm and the cross-head speed was 0.8 m/s. A multiple comparison with Fisher's least significance difference (LSD) method at $\alpha = 0.05$ was conducted with SAS 9.2 software (SAS Institute Inc. NC, USA).

2.3 Results and discussion

2.3.1 Fiber yields and chemical components

Figure 2.1 shows the yields and chemical components of the retted fibers and the raw kenaf bast.

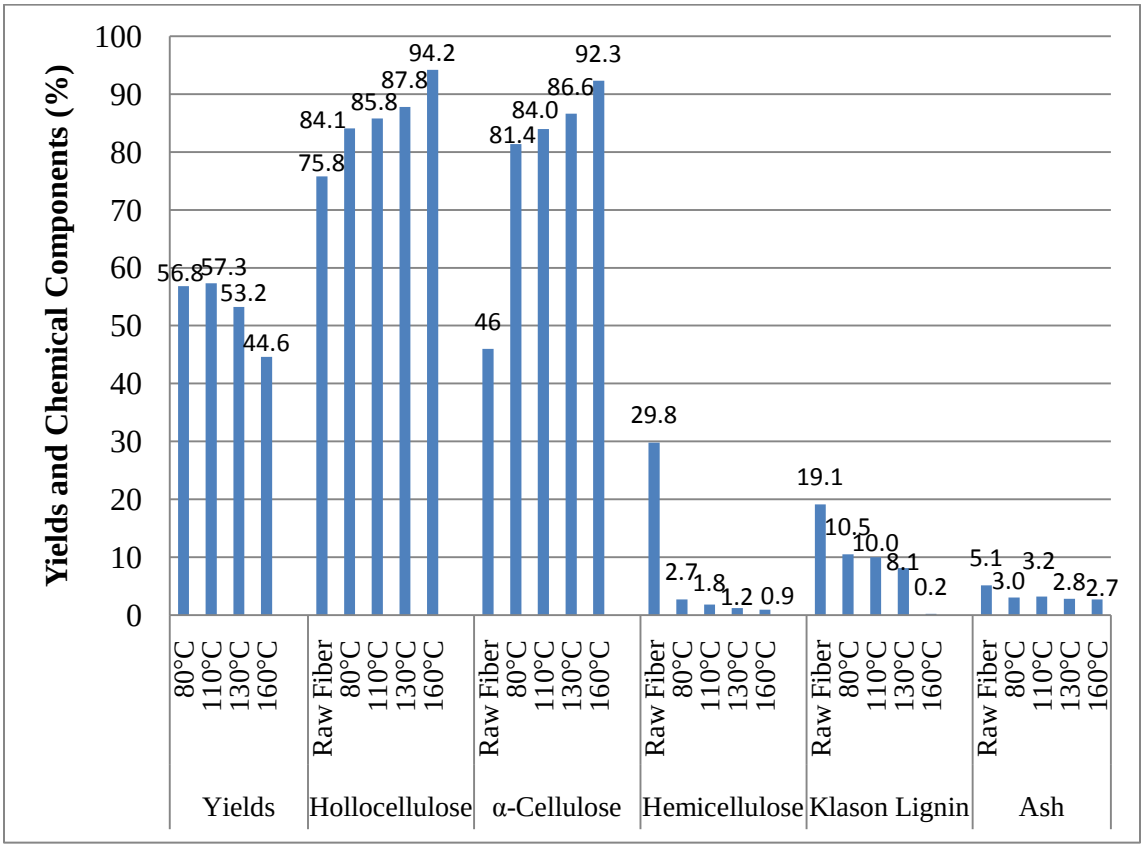

Figure 2.1 Yields and chemical components of the retted kenaf fibers.

The fiber yields gradually decrease as the retting temperature increases. This result can be attributed to the removal of lignin, hemicelluloses, and low molecular weight compounds. The hollocellulose contents gradually increase as the retting temperature increases. The same pattern was found in the change of the α-cellulose

contents. This relates to the significant decrease of the lignin and hemicelluloses contents. The results in Figure 2.1 indicate the alkaline retting process used in the study removed most proportions of lignin and hemicelluloses.

The reactions of carbohydrates in alkaline solution are well known (Green *et al*. 1997; Hon and Shiraishi 2000), and involve the cleavage of glycosidic bonds, peeling reactions, and stopping reactions. Hemicelluloses are highly degraded through peeling reactions. Peeling reactions describe the cleavage of glycosidic units adjacent to the end units containing carbonyl groups, by which sugars are removed one by one from the reducing end. The resultant monosaccharide fragments are converted to acidic compounds. Peeling reactions are terminated by stopping reactions which convert the reducing end group to carboxylic acid. The peeling reactions break the glycosidic linkages at the end of a molecular chain. The hydrolysis of glycosidic linkage can also occur at the middle of a molecular chain and generates new reducing ends. Glycosidic bonds linking different sugars have different susceptibilities to alkaline hydrolysis. For example, xylans are much more resistant to peeling reaction than glucomannans. Under 100 ℃, most xylans are dissolved. Above 100 ℃ peeling reactions also occur.

During alkaline retting, cellulose undergoes both peeling reactions and glycosidic hydrolysis. However, glycosidic cleavage is more important than peeling reaction. The degradation and solution of hemicelluloses in alkaline solution results in more weight loss than cellulose because hemicelluloses are more susceptible to chemicals than cellulose.

The degradation of lignin in alkaline conditions is well known (Bura and Gustafson 2010). In lignin, a quinone methide is readily formed when a free phenolic

hydroxyl connects with a benzene ring. The oxygen of the quinone group attracts the electron density on the double bond making the carbon more positive. This in turn shifts the electron densities of the other bonds on this conjugated system. The reduced electron density areas act as sites for nucleophilic attack because of their available electron pairs.

2.3.2 Surface morphology analysis

Figure 2.2 shows the visible appearances of the kenaf fibers that were retted at the four temperatures.

Figure 2.2 Images of the retted kenaf fibers. The labels mean the retting temperatures.

The kenaf fibers retted at 80 ℃, 110 ℃ and 130 ℃ were fiber bundles bigger and longer than those retted at 160 ℃. For the fibers retted at 80 ℃, 110 ℃, and 130 ℃, an

additional mechanical disintegration was applied to shorten and separate the fibers. Having been mechanically disintegrated, these fibers have the same distribution of length, diameter, and aspect ratio, because they went through the same mechanical disintegration process. The kenaf fibers retted at 160 ℃ were fine individual fibers and not subjected to mechanical disintegration.

The average and standard deviation of the dimensions are shown in Table 2.1.

Table 2.1 Average and standard deviation of the fiber dimensions.

		Length (μm)	Diameter (μm)	Aspect ratio
Mechanical disintegrated	Ave.*	1578.8	20.3	89.0
	Stdev.*	524.8	9.4	41.7
Retted at 160 ℃	Ave.	468.0	18.2	16.0
	Stdev.	575.5	6.4	15.1

*Ave. means average of the 70 samples. *Stdev. means the standard deviations.

The distributions of the fiber dimensions are shown in Figures 2.3, 2.4, and 2.5. The lengths of the mechanically disintegrated fibers ranged from 500 μm to 2,600 μm. The lengths of the fibers retted at 160 ℃ ranged from 54 μm to 868 μm, a much smaller range than the mechanically disintegrated fibers. The mechanically disintegrated fibers had aspect ratios ranging from 24 to 148, which were higher than those of the fibers retted at 160 ℃.

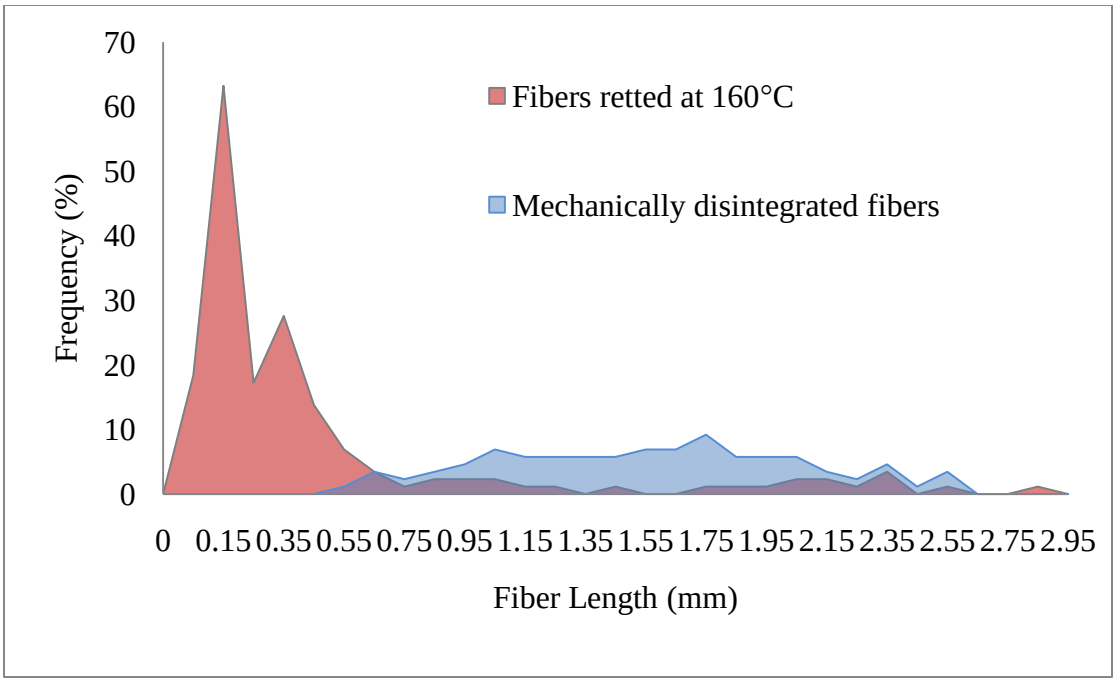

Figure 2.3 Length distributions of the retted kenaf fibers.

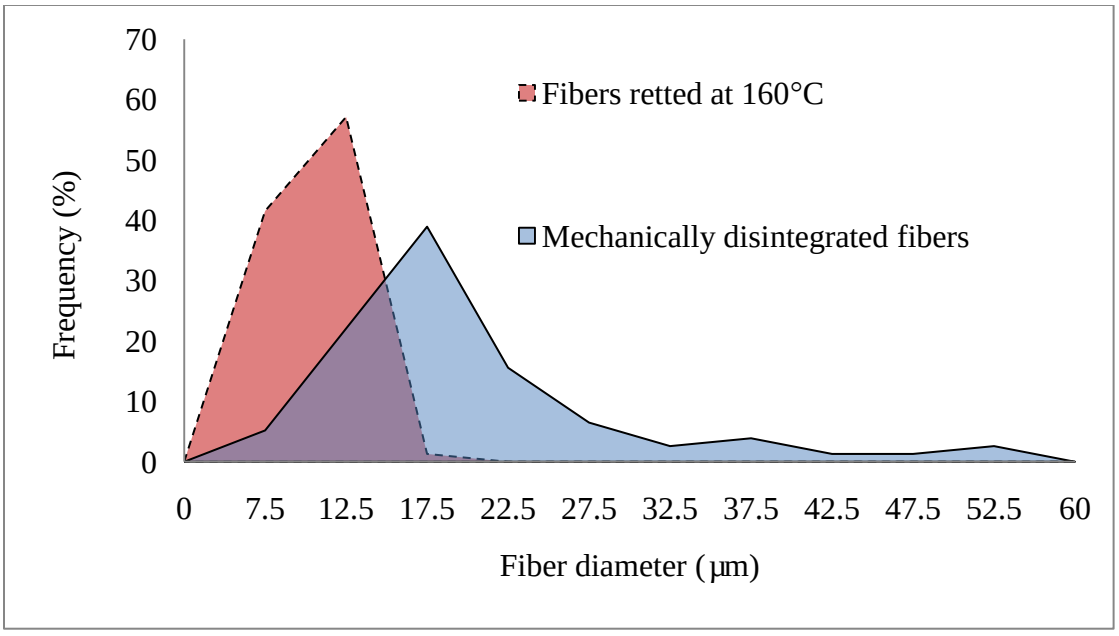

Figure 2.4 Diameter distributions of the retted kenaf fibers.

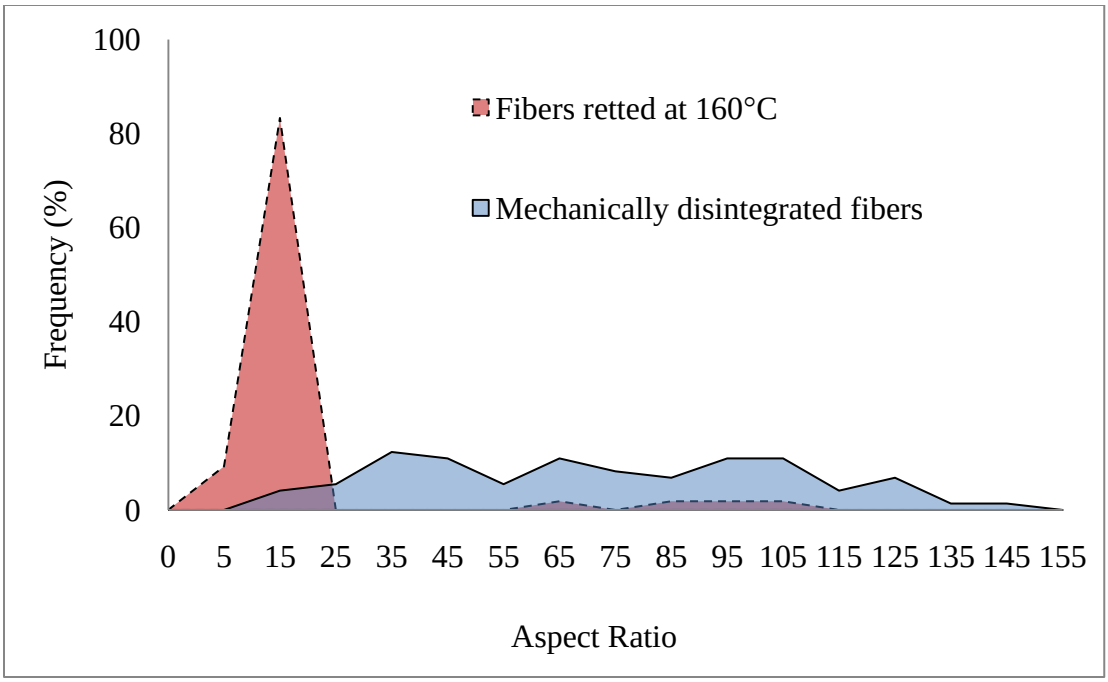

Figure 2.5 Aspect ratio distributions of the retted kenaf fibers.

Figure 2.6 shows the SEM images of the cell wall of the retted kenaf fibers. Micropores were generated in the cell wall of the fibers retted at 130 ℃ and 160 ℃. The generation of the micropores was due to the removal of hemicelluloses and lignin. The micropore size was about 50 nm. Lignin has three-dimensional structures. The maximum size of a lignin molecule can be estimated by assuming it is composed of two dimensional alignments of the monomers with a maximum degree polymerization. The minimum molecular size of a lignin monomer can be estimated as the diameter of a benzene ring, about 0.28 nm (Berresheim *et al*. 1999). A maximum degree polymerization of lignin is approximately 5000 (Holmgren 2008). Therefore, the maximum lignin molecular size can be estimated to be 1400 nm if the bond length is not counted. Removal of lignin could generate void space in nanometer scale.

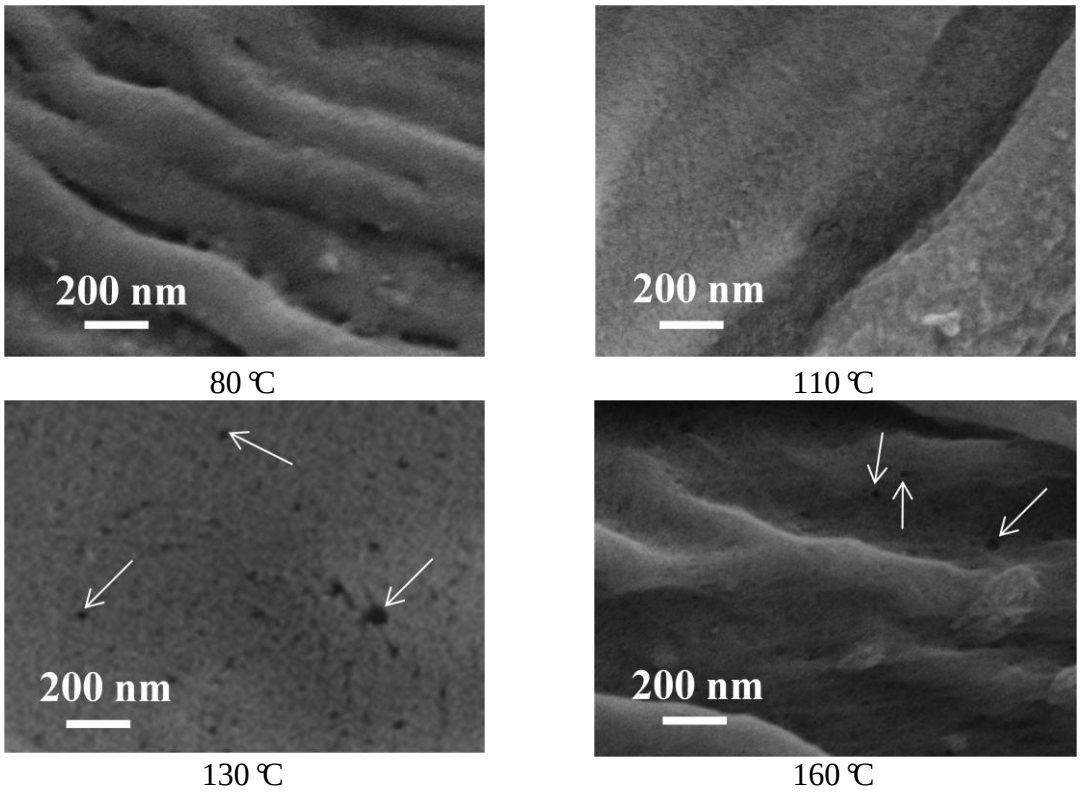

Figure 2.6 SEM images of the cell wall of the retted kenaf fibers. The labels mean the retting temperatures. Arrows designate the micropores.

The diameter of sugar monomers which compose hemicelluloses, e.g., glucose, xylose, mannose, galactose, rhamnose, and arabinose, is estimated as the molecular diameter of glucose—approximately 0.5 nm (Li 2002). The number of sugar monomers in a hemicellulose molecular backbone ranges from 70 to 200 (Saha 2003). Therefore, the length of a hemicellulose molecule is estimated to be 75 to 100 nm. Based on the calculation, it is reasonable that the removal of lignin and hemicelluloses generated nanometer scaled mciropores in the fiber cell wall.

2.3.3 Surface hardness and elastic moduli of the retted kenaf fibers

Figure 2.7 and 2.8 show the surface hardness and elastic moduli of retted kenaf fibers.

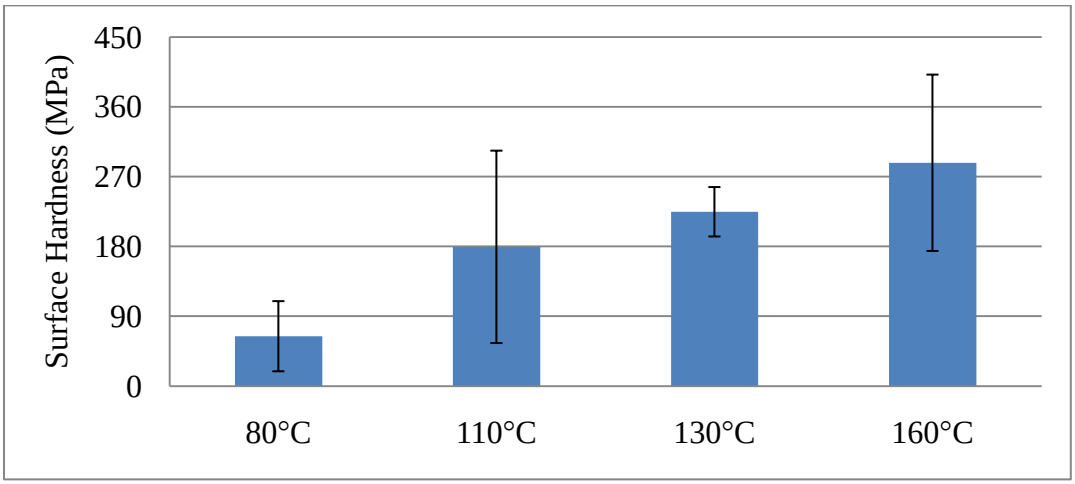

Figure 2.7 Surface hardness of the retted kenaf fibers. The labels mean the retting temperatures.

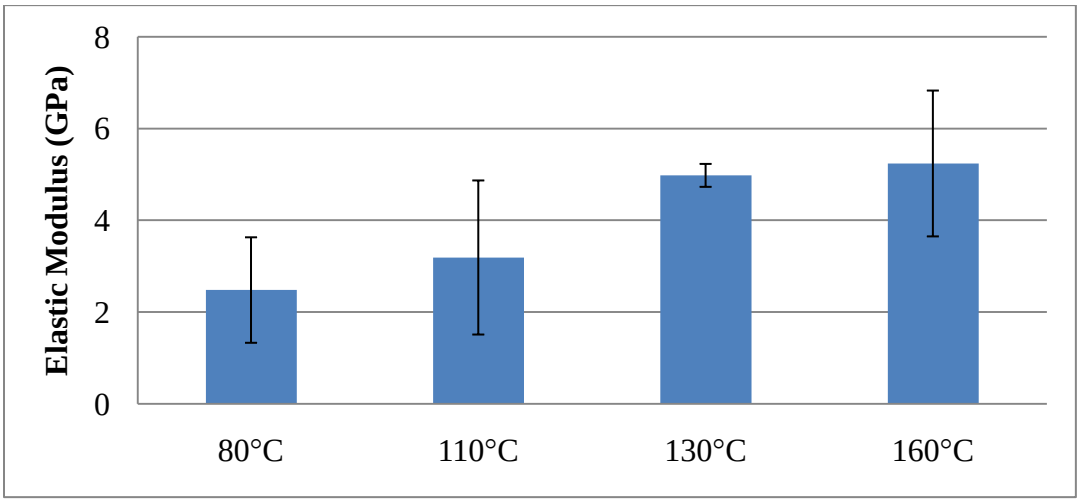

Figure 2.8 Elastic moduli of the retted kenaf fibers. The labels mean the retting temperatures.

The surface hardness and elastic moduli of the fibers increased as the retting temperature increased. The average elastic modulus and surface hardness of the fibers retted at 160 ℃ was two times higher and four times higher than that of the fibers retted at 80 ℃.

Compared with cellulose which is highly crystalline and strong, hemicelluloses have a random and amorphous structure with little strength. Although lignin has three-dimensional structures, lignin macromolecules degrade during alkaline retting process. The remaining lignin in the retted fibers should be low molecular weight compounds and lose the native stiffness. The surface mechanical properties mainly depend on the cellulose content of the retted fibers.

The hardness of cellulose is governed by the highly crystallized structure in crystalline regions, and the hydrogen bonds in cellulose structures (Lahiji *et al*. 2010; Li 2002). The cellulose I structure exists in native cellulose plants. However, under heat and alkali, cellulose I converts to a cellulose II structure which is more thermodynamically stable (Kono and Numata 2004; Klemm *et al*. 2005).

Kovalenko (2010) studied the hydrogen bonds in the cellulose II structures. The origin and center chains form the corresponding alternating planar sheets, in which the chains are linked to each other by intermolecular hydrogen bonds, viz., by the O(6)H-O(2) hydrogen bonds in the sheets of the origin chains and by the O(2)H-O(6) hydrogen bonds in the sheets of the center chains. Among intramolecular hydrogen bonds, there are O(3)H-O(5) bonds between adjacent glucopyranose units. The number of the bonds (four hydrogen bonds per glucopyranose residue) is sufficiently large to have an effect on the properties of cellulose II. The cellulose macromolecule is highly rigid due to the

presence of a three-dimensional hydrogen bond network, in addition to the C-O-C bonds between the glucopyranose rings. There is only the O(3)H-O(5) hydrogen bond between the pyranose rings. However, in cellulose II the absence of the second hydrogen bond along the chain is compensated by the presence of four weak hydrogen bonds between the sheets, which provides the more uniform (three-dimensional) distribution of the hydrogen bond network.

Elastic deformation of cellulosic fibers involves the stretching of the hydrogen bonds in cellulose. Hydrogen bonds are not broken and are recoverable when the stress is removed during elastic deformation. High energy is required to induce permanent deformation by breaking the hydrogen bonds in the cellulose crystallite. Therefore, both the surface hardness and elastic moduli of the retted fibers increase as cellulose content increases.

There were large variations in the results. This was caused by the non-homogeneous distribution of chemical compositions and structures. The indenter tip had a diameter of only 50 nm, and the indentation depth was only several hundred nanometers. The compositions at the indentation locations may be different from time to time. For example, the results are different if the tip located on decomposed compound of lignin compared with that located on a cellulose crystallite. The results are also different if the center of the tip is at an amorphous region of cellulose compared with that at a crystalline region. The micropore distribution in the fiber cell wall is not uniform. Some indentations may locate at a micropore but have no cell wall mass. The result would be lower than that at cell wall mass. The microscope attached to the testing

equipment cannot give clear magnified images of the fibers. This makes it difficult to select proper indentation locations.

2.3.4 Tensile properties of the retted kenaf fibers

The tensile properties of the individual fibers retted at 110 ℃ and 160 ℃ are shown in Figure 2.9. There are significant differences in the tensile properties, including tensile moduli and tensile strengths, between the fibers retted at 110 ℃ and 160 ℃. The tensile modulus of the fibers retted at 110 ℃ was 10.1 GPa higher than that of the fibers retted at 160 ℃. The fiber tensile strength dropped from 1051 MPa to 810 MPa as the retted temperature increased from 110 ℃ to 160 ℃.

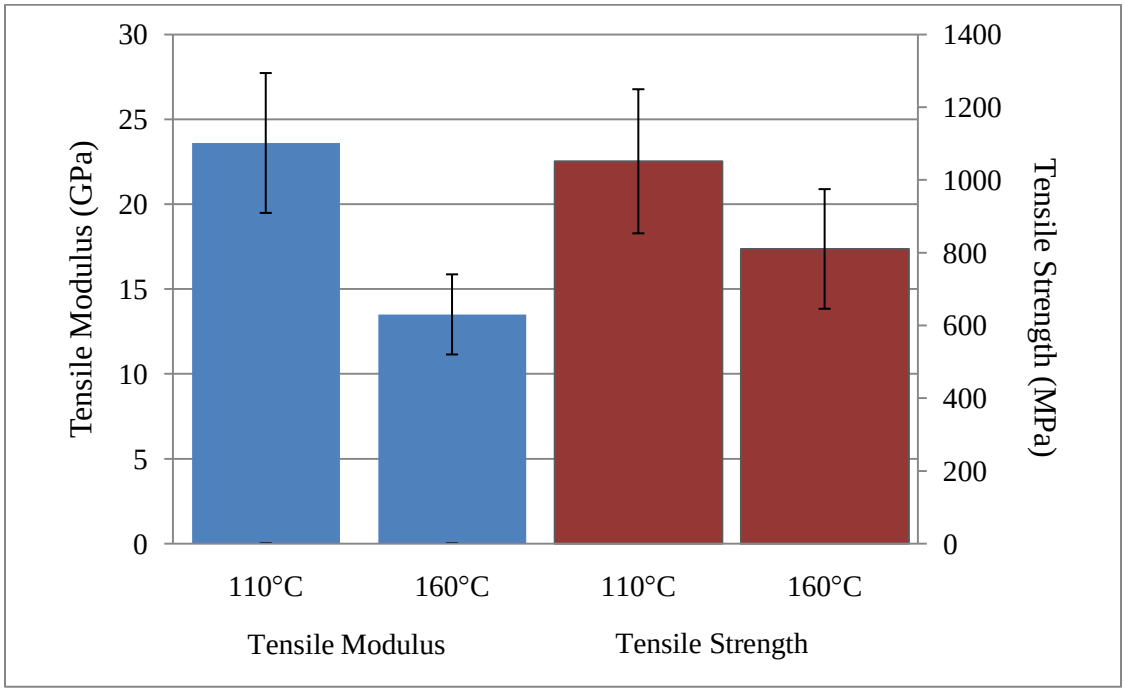

Figure 2.9 Tensile properties of the individual retted kenaf fibers. The labels mean the retting temperatures.

The morphology analysis discussed above shows that micropores were generated in the cell wall of the fibers retted at 160°C because of the removal of lignin and hemicelluloses. The micropores could act as cracks and initiate tensile failure during tensile testing. With the absence of lignin and hemicelluloses, there was no matrix transferring stress from one cellulose microfibril to another. The microfibrils may separate at a low tensile stress, and the deformation is unrecoverable. However, 1.8% of hemicelluloses and 10% of lignin remained in the fibers retted at 110°C. Lignin filled the spaces in the cell wall between cellulose and hemicelluloses, and covalently linked to the hemicelluloses and crosslinking the different polysaccharides (Chabannes *et al*. 2001). Hemicelluloses connected with cellulose with both covalent bonds and hydrogen bonds (Albersheim *et al*. 2010). Lignin and hemicelluloses transferred stress and conferred mechanical strength to a whole fiber. The tensile strengths and moduli of the fibers retted at 110°C were significantly higher than those of the fibers retted at 160°C.

2.4 Conclusions

The hermetical alkaline retting process effectively removed lignin and hemicelluloses from kenaf bast at 160°C. The α-cellulose content of the fibers retted at 160 ℃ was 92%. Higher retting temperatures resulted in higher surface hardness and elastic moduli of the retted kenaf fibers. Micropores were generated in the cell wall of the fibers retted at 130 ℃ and 160 ℃, providing the possibility of anchoring inorganic nanoparticles in the cell wall.

CHAPTER III

INORGANIC NANOPARTICLE IMPREGNATION TECHNOLOGY

3.1 Materials

Kenaf bast was harvested from the Mississippi State University (MSU) North Farm in January 2007. The bast was cut into 50.8 mm lengths. The moisture content was 8.1% before the retting process was applied. Sodium hydroxide (NaOH) aqueous solution (5%) was prepared with distilled water and NaOH beads (Lab grade, Thermo Fisher Scientific Inc.). Acetic acid (17.4N, Reagent grade, Thermo Fisher Scientific Inc.) was used to adjust pH value of the retting liquid. Sodium carbonate (Na_2CO_3) aqueous solutions (0.1 mol/L) and calcium chloride ($CaCl_2$) aqueous solutions (0.1 mol/L and 0.2 mol/L) were prepared using distilled water. The sodium carbonate and calcium chloride were supplied by Fisher Scientific Inc.

3.2 Methods

3.2.1 Inorganic nanoparticle impregnation (INI) treatments

The flowchart for the INI treatments procedure is shown in Figure 3.1 (Lee *et al*. 2007; Shi *et al*. 2007 and 2008).

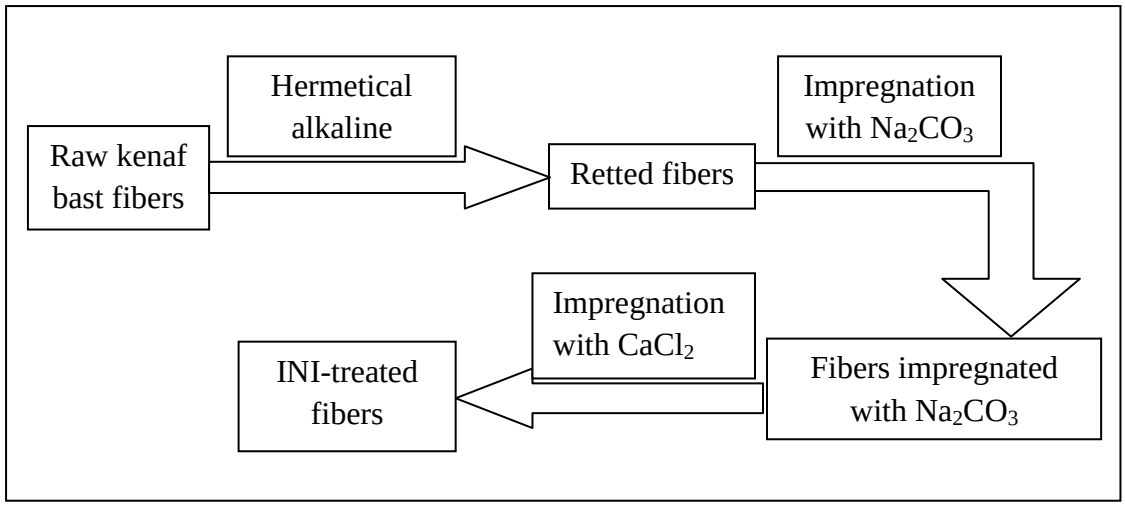

Figure 3.1 Flowchart of the INI treatments.

Kenaf bast was retted with a 5% NaOH solution (fiber: NaOH solution = 1:30, g/ml) in a hermetical reactor (Parr Instrument Co. 251M) at 160 ℃. The retting process took one hour and was aided with a mechanical stirring. The autogeneous vapor pressure was 0.60 MPa. After retting, the pH of the retting liquid and retted fibers was adjusted to 7.0 using acetic acid. The neutralized fibers were washed with water to remove chemicals from the fibers. These fibers retted at 160 ℃ were used as the control fibers in this chapter. The control fibers and 0.1mol/L Na_2CO_3 aqueous solution (fiber: solution = 5: 400, g/ml) were mixed in the hermetic reactor with mechanical stirring at 70 ℃ for 30 minutes. The autogeneous vapor pressure was 0.1 MPa. The excess ions (CO_3^{2-} and Na^+) were washed away from the fibers using distilled water. The fibers and $CaCl_2$ aqueous solution were mixed in the hermetic reactor with mechanical stirring for 15 minutes. The $CaCl_2$ solution was impregnated and the reaction between $CaCl_2$ and Na_2CO_3 occurred in the fibers at three different temperatures and autogeneous vapor

pressures ((1) 100℃, 0.15MPa; (2) 130℃, 0.30 MPa; and (3) 160℃, 0.70 MPa). The molar ratios of Na_2CO_3 to $CaCl_2$ were 1:1 and 1:2 through the use of two concentrations of $CaCl_2$ solutions, 0.1 mol/L and 0.2 mol/L. Six reaction conditions were used including three temperatures and two molar ratios. These are shown in Table 3.1.

Table 3.1 Six reaction conditions for INI treatments.

No.	Temperatures (℃)	Vapor Pressures (MPa)	Molar ratios of Na_2CO_3 to $CaCl_2$
1	100	0.15	1:1
2	100	0.15	1:2
3	130	0.30	1:1
4	130	0.30	1:2
5	160	0.70	1:1
6	160	0.70	1:2

After the impregnation of the two ionic solutions, $CaCO_3$ particles were synthesized by the reaction between Na_2CO_3 and $CaCl_2$ in the fiber's cell wall and on the fiber surface. Excess ionic precursors and the free $CaCO_3$ particles on the fiber surface were washed away with water.

3.2.2 Determination of $CaCO_3$ loading weight percentages

Control fibers and INI-treated kenaf fibers (1.5 g for each type of fibers) were exactly weighed and burned in the furnace. The decomposition of $CaCO_3$ was complete under this experimental condition (Gordon 1969). The ash weight from the INI-treated fiber was composed of fiber ash and CaO. The ash weight from control fiber was only the fiber ash. Therefore, the weight percentages of $CaCO_3$ can be calculated by equation (3.2).

$$CaCO_3 \xrightarrow{\text{Heat}} CaO + CO_2 \quad (3\text{-}1)$$

Control fibers and INI-treated kenaf fiber (1.5 g for each type of fibers) was exactly weighed and burned in furnace. The decomposition of $CaCO_3$ was complete under this experimental condition (Gordon 1969). The ash weight from the INI-treated fibers was composed of fiber ash and CaO. The ash weight from control fibers was only the fiber ash. Therefore, the weight percentages of $CaCO_3$ can be calculated by equation (3-2).

$$CaCO_3 \text{ Loading } (\%) = \frac{WA_{\text{INI Fiber}} - WA_{\text{Control fiber}}}{W_{\text{INI Fiber}}} \times \frac{100.0875}{56.0778} \times 100\% \quad (3\text{-}2)$$

where: $WA_{\text{INI Fiber}}$ = the weight of ash containing in INI-treated fiber;

$WA_{\text{Control Fiber}}$ = the weight of ash containing in control fiber;

$W_{\text{INI Fiber}}$ = the initial weight of INI-treated fiber;

100.0875 = the molecular weight of $CaCO_3$;

56.0778 = the molecular weight of CaO.

3.2.3 Surface morphology and elemental analysis

A Zeiss SupraTM 40-Gemini® Scanning Electron Microscope (SEM) was used to study the morphology of the INI-treated kenaf fibers with an accelerating voltage of 15 kV. The fibers were coated by gold sputtering to give a 15 nm thick before being scanned using SEM. Elemental determination was conducted using a Bruker Quantax 200 X Flash Energy-Dispersive X-ray Spectrometer (EDS) System (LN2-free high speed 30mm2 SDD Detector).

3.2.4 Surface hardness and elastic modulus testing

A Hysitron TriboIndenter with a Berkovich diamond tip was used to test the fiber surface hardness and elastic moduli at a 400 μN peak force and a 40 μN/s loading rate using a 10 second segment time. The INI-treated kenaf fibers were mounted in a hardened epoxy matrix, and the load was perpendicular to the longitudinal direction of the fibers. According to the elastic punch theory and Oliver and Pharr's method (1992), the reduced elastic moduli can be obtained based on the elastic contact stiffness.

3.3 Results and discussion

3.3.1 $CaCO_3$ loading weight percentages

Figure 3.2 shows the loading weight percentages of $CaCO_3$ in the INI-treated kenaf fibers.

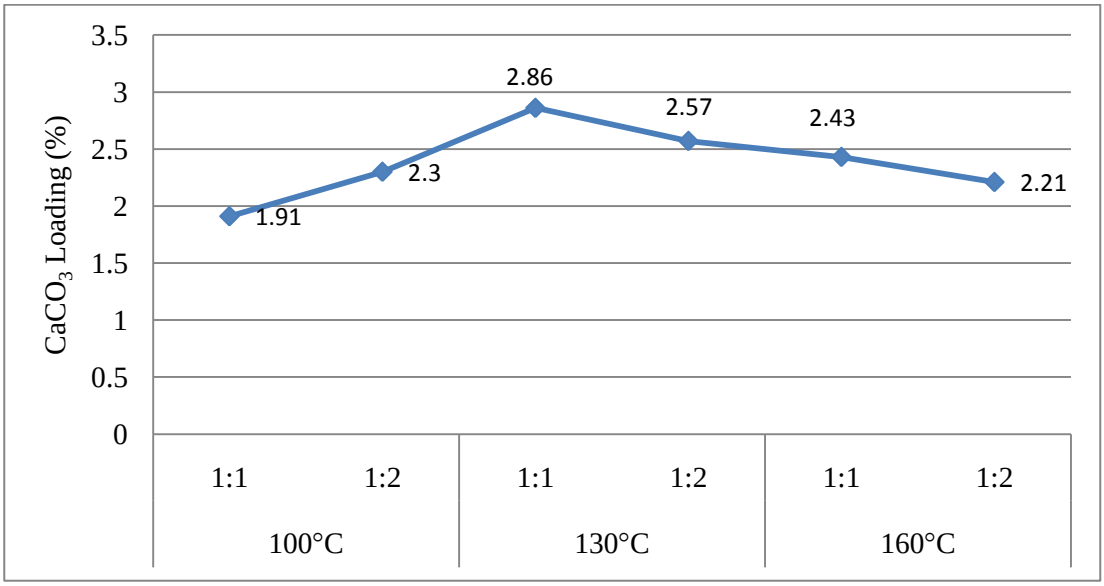

Figure 3.2 Weight percentages of $CaCO_3$ loading of INI-treated kenaf fibers. The labels mean the molar ratios of Na_2CO_3 to $CaCl_2$ and the reaction temperatures.

The determination of the weight percentages of $CaCO_3$ loading was repeated twice for each type of the fiber. The errors were less than 0.1%. The fibers treated at 130 ℃ (Na_2CO_3 : $CaCl_2$=1:1, mol:mol) yielded the highest $CaCO_3$ loading.

3.3.2 Surface morphology and elemental analysis

Figure 3.3 shows the SEM images of the INI-treated kenaf fibers.

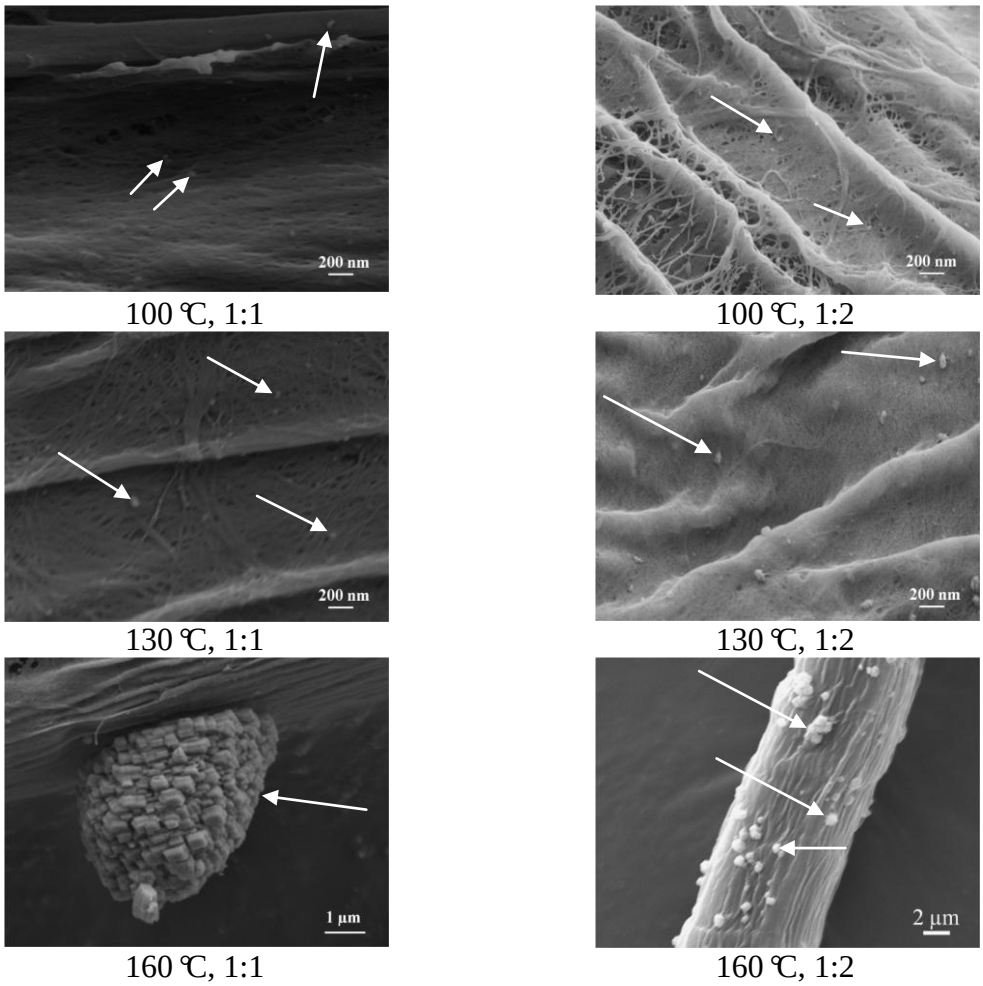

Figure 3.3 SEM images of INI-treated kenaf fibers. 1:1 and 1:2 means the molar ratios of Na_2CO_3 to $CaCl_2$. The temperatures mean the reaction temperatures. The arrows designate $CaCO_3$ particles.

As the temperature increased, the size of $CaCO_3$ particles increased, indicating temperature played an important role in the formation of $CaCO_3$ particles. High temperature may accelerate the formation of $CaCO_3$ particles. The sizes of the $CaCO_3$ nanoparticles in the fibers treated at 130 ℃ were smaller than 90 nm. However, in the fibers treated at 160 ℃, the size of some $CaCO_3$ particles grew over 1 μm. From the SEM images of the INI-treated kenaf fibers, more $CaCO_3$ particles with bigger size were observed on the surface of the fibers treated at 160°C than the fiber treated at 130°C. However, the $CaCO_3$ loading weight percentage at 160°C is lower than that at 130°C (Figure 3.2). This may be because the formation of $CaCO_3$ crystals was quicker at 160°C than that at 130°C. At 160°C, the reaction may occur on the fiber surface or at a slight depth in the fiber cell wall. $CaCO_3$ nucleation started and the crystal size grew quickly. The resultant $CaCO_3$ particles blocked Ca^{2+} from penetrating deeply. The formation of $CaCO_3$ occurred on the fiber surface and at a slight depth in the fiber cell wall. The interlocking mechanism kept the $CaCO_3$ particles from washing away. The $CaCO_3$ loading weight percentage at 160°C is not higher than at 130°C, although the particle size is bigger. Comparatively, the growth of $CaCO_3$ crystals may be slower at 100°C and 130°C, and Ca^{2+} could impregnate deeper through the micropores in the fiber cell wall and the formation of $CaCO_3$ could occur in the fiber cell wall.

The EDS spectra of the control fiber and INI-treated (160°C, 1:1) kenaf fiber are shown in Figures 3.4 and 3.5. In the control fiber, a trace of calcium (Ca) and magnesium (Mg), which took atomic percentages of 0.27% and 0.07% respectively, were detected. The trace of Ca and Mg in the control fiber may come from contamination. A high percentage of Ca (13.22%) was detected in the INI-treated kenaf

fibers. Carbon (C) and oxygen (O) were detected from the INI-treated kenaf fibers also. In the INI-treated kenaf fiber, Ca may exist as calcium ion (Ca^{2+}) with Cl^- ion or as $CaCO_3$. However, neither sodium (Na) nor chlorine (Cl) was detected. Therefore, Ca can only exist as $CaCO_3$. This evidence supports the reaction between Na_2CO_3 and $CaCl_2$, and the synthesis of $CaCO_3$. The byproduct, NaCl, was washed away after the INI treatments. Peaks for palladium (Pd) between 1.5 and 2.5 keV came from the specimen coating and were not counted.

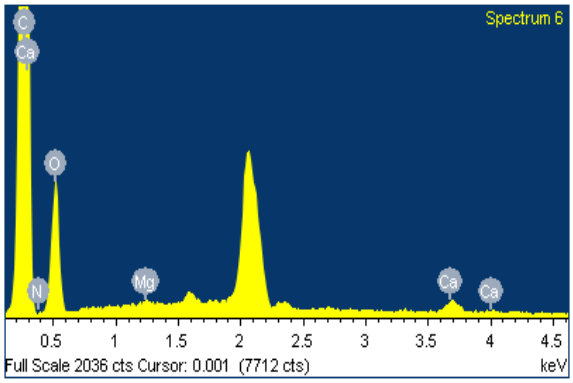

Elements	Weight, %	Atomic, %
C	64.97	70.48
N	12.38	11.51
O	21.69	17.67
Mg	0.12	0.07
Ca	0.83	0.27
Totals	100.00	100.00

Figure 3.4 EDS spectrum of the control fiber.

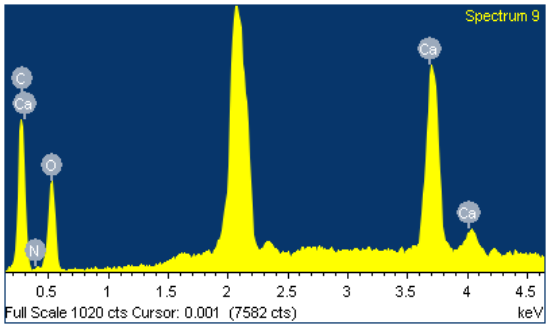

Element	Weight, %	Atomic, %
C	24.03	35.15
N	8.52	10.68
O	37.29	40.95
Ca	30.17	13.22
Totals	100.00	100.00

Figure 3.5 EDS spectrum of INI-treated kenaf fiber.

3.3.3 Surface hardness and elastic moduli of the INI-treated kenaf fibers

Figure 3.6 and 3.7 show the surface hardness and elastic moduli of the INI-treated kenaf fibers.

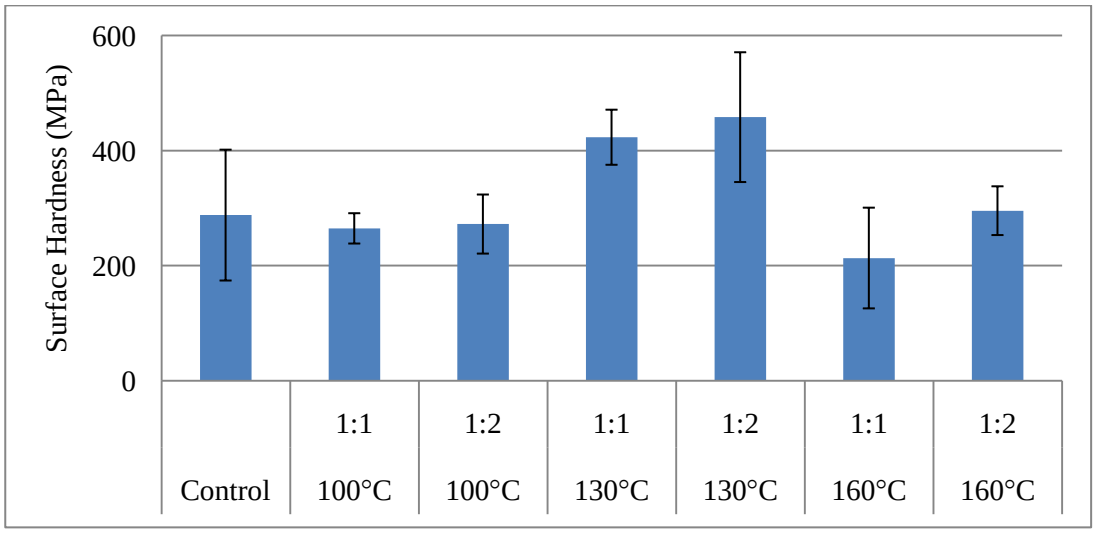

Figure 3.6 Surface hardness of the INI-treated kenaf fibers. The labels mean the molar ratios of Na_2CO_3 to $CaCl_2$ and the reaction temperatures.

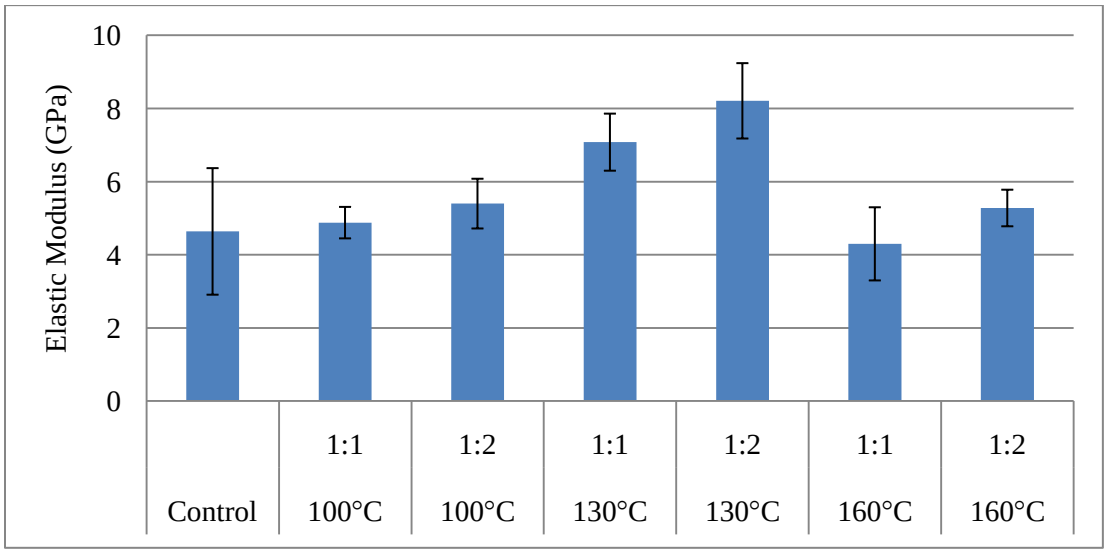

Figure 3.7 Elastic moduli of the INI-treated kenaf fibers. The labels mean the molar ratios of Na_2CO_3 to $CaCl_2$ and the reaction temperatures.

The fibers treated at 130 ℃ yielded a 52.6-76.9% increase in modulus and a 47.0-59.1% increase in surface hardness compared with control fibers.

$CaCO_3$ crystal has much higher surface hardness (1.5-4.7 GPa) and elastic modulus (73.5-85.5 GPa) (Presser *et al*. 2010) than kenaf bast fibers. Sufficient $CaCO_3$ loaded in the fiber cell wall theoretically could enhance the fiber surface hardness and elastic modulus. The displacement of the indentation in this study was several hundred nanometers. This distance is quantitatively larger than the width of a cellulose crystallite. The indentation was perpendicular to the axis and along the direction of the width of cellulose molecular chains. Therefore the material supporting the cellulosic fibers against the indentation greatly influenced the testing results. The fibers treated at 130℃ gave the highest $CaCO_3$ loading. As discussed, the $CaCO_3$ particles concentrated in fiber cell wall. When the fiber mass was indented, $CaCO_3$ particles which filled in the micropores in fiber cell wall may have provided a mechanical support for the fiber mass, thus contributing to the high surface hardness and elastic modulus. Large variations were observed here also. This resulted from the non-homogeneous distribution of $CaCO_3$ particles, cellulose structure, and indentation locations.

It has been discussed above that 160℃ may be too high and results in a shallow impregnation of Ca^{2+}, thus the distribution of $CaCO_3$ particles concentrated at a slight depth in the fiber cell wall and some $CaCO_3$ particles exposed on the fiber surface. However, during the preparation of nanoindentation samples, a certain depth of fiber cell wall was milled off until the inner part of the fiber cell wall was exposed. For the fibers treated at 160℃, it is likely that some $CaCO_3$ particles were milled away from the fiber surface before indentation testing. This may be the reason the surface hardness and

elastic modulus of the fibers treated at 160°C were not significant different from those of the control fibers.

Less $CaCO_3$ was loaded in the fiber cell wall at 100°C than at 130°C (Figure 3.3.) The micropores were still obvious in the fibers treated at 100°C (Figure 3.3). It can be concluded that $CaCO_3$ in the fibers treated at 100°C was not sufficient to enhance the fibers surface hardness and elastic modulus. Moreover, the $CaCO_3$ particle distribution is not condensed in the fibers treated at 100°C. There is no guarantee the indentation could locate at an area where $CaCO_3$ exists. Therefore, there is no significant difference in surface hardness and elastic modulus between the fibers treated at 100°C and control fibers.

3.4 Conclusions

$CaCO_3$ particles were successfully impregnated in the micropore structure of the fiber cell wall. Reaction temperature plays an important role in accelerating the synthesis of $CaCO_3$ particles. INI treatment at 130℃ resulted in the improvements in the fiber surface hardness by 53-77% and the elastic modulus by 47-59%, compared to the control fibers.

CHAPTER IV

PREPARATION OF CELLULOSE NANOWHISKERS

4.1 Materials

Kenaf bast was harvested from the Mississippi State University (MSU) North Farm in January 2007. The bast was cut into 50.8 mm lengths. The moisture content was 8.1% before the retting process was applied. Sodium hydroxide (NaOH) aqueous solution (5%) was prepared with distilled water and NaOH beads (Lab grade, Thermo Fisher Scientific Inc.). Acetic acid (17.4N, Reagent grade, Thermo Fisher Scientific Inc.) was used to adjust pH of the retting liquid. Hydrogen peroxide (H_2O_2, 37%) solution and sulfuric acid (H_2SO_4, 98%) solutions were diluted to 10% and 30%, respectively. All of the chemicals were purchased from Fisher Scientific Inc.

4.2 Methods

4.2.1 Preparation of CNWs

Kenaf bast was retted in a 5% NaOH solution at 160 ℃ for one hour. A hermetic reactor was used, in which autogeneous vapor pressure (0.60 MPa) was achieved. Then the pH of the retting liquid and the fibers was adjusted to 7.0 using acetic acid, and the retted fibers were washed with water to remove the chemicals from the fibers. The retted fibers were then bleached with 10% H_2O_2 at 70 ℃ for 1 hour. Acid hydrolysis of the

bleached fibers was then conducted with 30% H_2SO_4 at 80℃ for four hours. A mechanical stirring was applied using a laboratory stirrer (IKA RW 16 basic) to aid the hydrolysis of the fibers. The rotation speed was 1200 rpm. An acidic suspension of microfibers and CNWs was obtained. The acidic liquid was removed by repeating centrifugation and replacing the acidic liquid with fresh distilled water. The centrifugation was conducted with an Eppendorf Centrifuge (Model 5810) at a rotating speed of 6,500 rpm for five minutes. The microfibers and CNWs were both precipitated and could not be separated until the pH of the suspension reached approximately 6.0. The supernatant acidic liquid was removed, and fresh distilled water was added to dilute the remaining acid. The process was repeated until the suspension was neutralized. The suspension was put into a centrifuge with a rotation speed of 7,600 rpm. The milk-like CNW supernate was separated from the microfiber sediments. The separation was repeated until the supernatant liquid was clear. The CNW suspension was sonicated for ten minutes using a Cole-Parmer ultrasonic processor with a CV33 converter and a 13mm probe (750 watts, 20 kHz, 40% amplitude of vibration). The samples of retted fibers, bleached fibers, microfibers, and CNWs were freeze-dried before characterization.

4.2.2 Determination of fiber yields and chemical components

Chemical components, including holocellulose, α-cellulose, Klason lignin, and ash content were determined for raw kenaf bast, retted fibers, bleached fibers, microfibers and CNWs. The ash contents were measured using the TAPPI standard T 211-om. 93 (TAPPI 1993). The determination of Klason lignin was based on the constituent insoluble in 72% sulfuric acid, which was estimated in accordance with method No. 482 of the Institute of Paper Chemistry (1951). Holocellulose, the total polysaccharide

fraction (cellulose and hemicelluloses) of the fibers, was estimated according to the method used by Wise *et al*. (1946). α-Cellulose is the part of cellulose which does not dissolve in 17.5% sodium hydroxide solution and was determined in accordance with the method from the German Association of Cellulose Chemists and Engineers (1951). The yields of retted fibers were obtained based on the ratio of the oven-dry weights of the resultant fibers to the original weight of the raw kenaf bast.

4.2.3 Surface morphology analysis

The samples of retted fibers, bleached fibers, and microfibers were coated with gold to provide electrical conductivity. Scanning electron microscopy (SEM, Zeiss Supra TM 40) was used to analyze fiber morphology with an accelerating voltage of 15 kV. Seventy fibers were randomly chosen. Their dimensions were measured using Smart SEM User Interface software. The CNW samples for morphology analysis were obtained by placing a drop of the CNW suspension onto a microscope grid and drying it in air at ambient temperature. The dried samples were examined with a transmission electron microscope (TEM, JEOL JEM-2000 EX-II) at an accelerating voltage of 100 kV. The dimensions of seventy randomly chosen CNWs were measured from the TEM images.

4.2.4 Functional group analysis

The fiber samples were located at the stage of a Thermo Scientific Nicolet 6700 spectrophotometer. Infrared irradiated on the fiber samples. Fourier transform infrared (FT-IR) spectra were recorded. Functional groups of the fibers were studied through the FT-IR spectra.

4.2.5 Determination of the fiber crystallinity

The crystallinities of all fiber samples were measured using a Rigaku SmartLab X-ray Diffraction System with an operating voltage of 40 kV and a current of 44 mA. The fiber crystallinities (X_{CR}) were calculated by the Segal method (Segal 1959) as shown in Equation (4-1).

$$X_{CR} = \frac{I_{200} - I_{AM}}{I_{200}} \times 100\% \quad (4\text{-}1)$$

where: I_{200} is the height of the peak between 20˚ and 25˚, representing both the crystalline and amorphous regions; I_{AM} is the lowest height between 15˚ to 22.7˚, representing the amorphous regions only.

4.3 Results and discussion

4.3.1 Hierarchical yields and chemical components

The fiber yields and chemical components are shown in Figure 4.1. Alkaline retting removed most of the lignin and hemicelluloses from the kenaf bast fibers. A fiber yield of 44.6% was obtained after the alkaline retting. The α-cellulose content of the raw kenaf bast fibers was 45.95%, which was close to the yield of the retted fibers. This suggested the components remaining in the fiber after retting were mainly α-cellulose, as verified by the chemical component.

Bleaching eliminated the chromophoric groups in the retted fibers. Some cellulose molecular chains were also broken during bleaching. A 41.4% fiber yield was obtained after bleaching. The bleached fibers were hydrolyzed with sulfuric acid. Glycosidic bonds were broken within the amorphous regions of cellulose molecular chains. The percentage of the crystalline region increased, while the fiber size was

reduced by the acid hydrolysis. Some fibers were converted to be individual CNWs, while others were microfibers. The yield of CNWs was 10.4%, while the yield of microfiber was 26.3%. Considering that the 10.4% CNWs were obtained from α-cellulose, which made up 45.95% of the raw kenaf bast (Figure 4.1), about 22.6% of the α-cellulose had been converted into CNWs.

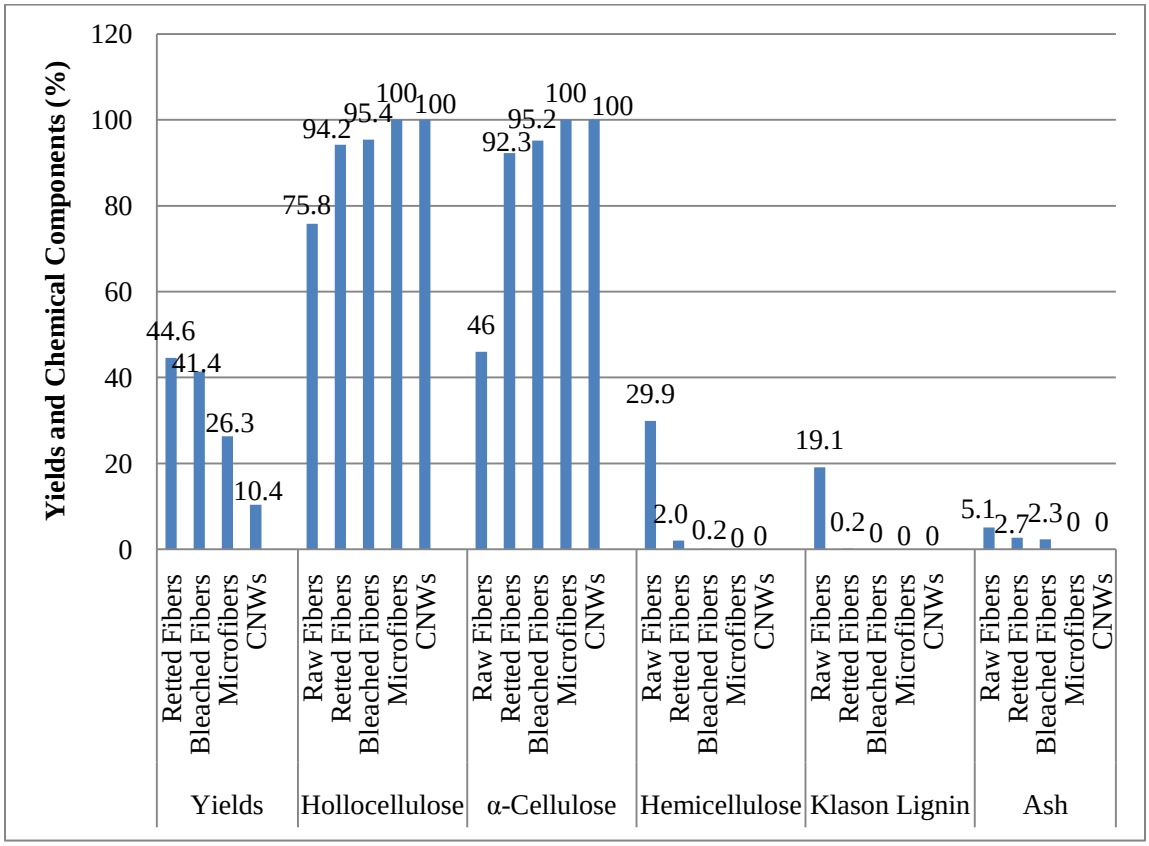

Figure 4.1 Yields and chemical components of the hierarchical fibers.

A small fraction of hemicellulose and lignin remained in retted fibers. Bleaching produced cellulosic fibers that contained only 0.2% hemicellulose and were totally free from Klason lignin. Bhatnagar (2005) reported the average hemicellulose contents of the

flax bast fiber and hemp fiber after acid hydrolysis and alkali treatment were 1 to 2%, and their average lignin content was 3%. Compared with that study, the alkali retting and bleaching used in this study were more effective for removing lignin and hemicelluloses.

The delignification mechanism of H_2O_2 under alkaline conditions has been studied (Hocking *et al*. 1977, 1994). The addition of NaOH in the bleaching system accelerated the dissociation of H_2O_2. Perhydroxyl ions (HOO^-), which were strong nucleophiles, were formed. This anion attacked ethylenic and carbonyl groups present in lignin. The fibers were bleached because of the elimination of the chromophoric groups. The resultant products can be degraded in sulfuric acid and this degradation will not result in insoluble residue in the subsequent procedure.

Acid hydrolysis severely cleaved β-1-4-glycosidic bonds (Xiang *et al*. 2003). The reaction began with a protonation of the glycosidic oxygen between two sugar units. Then the C-O bond was cleaved generating a cyclic carbonium ion. With the addition of water, a free sugar and a proton were liberated. Acid hydrolysis of cellulose resulted in weight loss because of the formation and removal of the resultant free sugars. The cleavage of glycosidic bonds occurred within amorphous regions. Therefore, the percentages of amorphous regions in the resultant microfibers and CNWs dropped markedly.

Crystalline regions of cellulose molecular chains were much more resistant to chemical attack than amorphous regions because of their highly ordered structures. Hemicelluloses have only amorphous structures and are susceptible to acid hydrolysis. Therefore, the microfibers and CNWs prepared from acid hydrolysis are pure cellulose.

4.3.2 Surface morphology analysis

Figure 4.2 shows the SEM images of the raw kenaf bast, retted fiber, bleached fiber and microfibers.

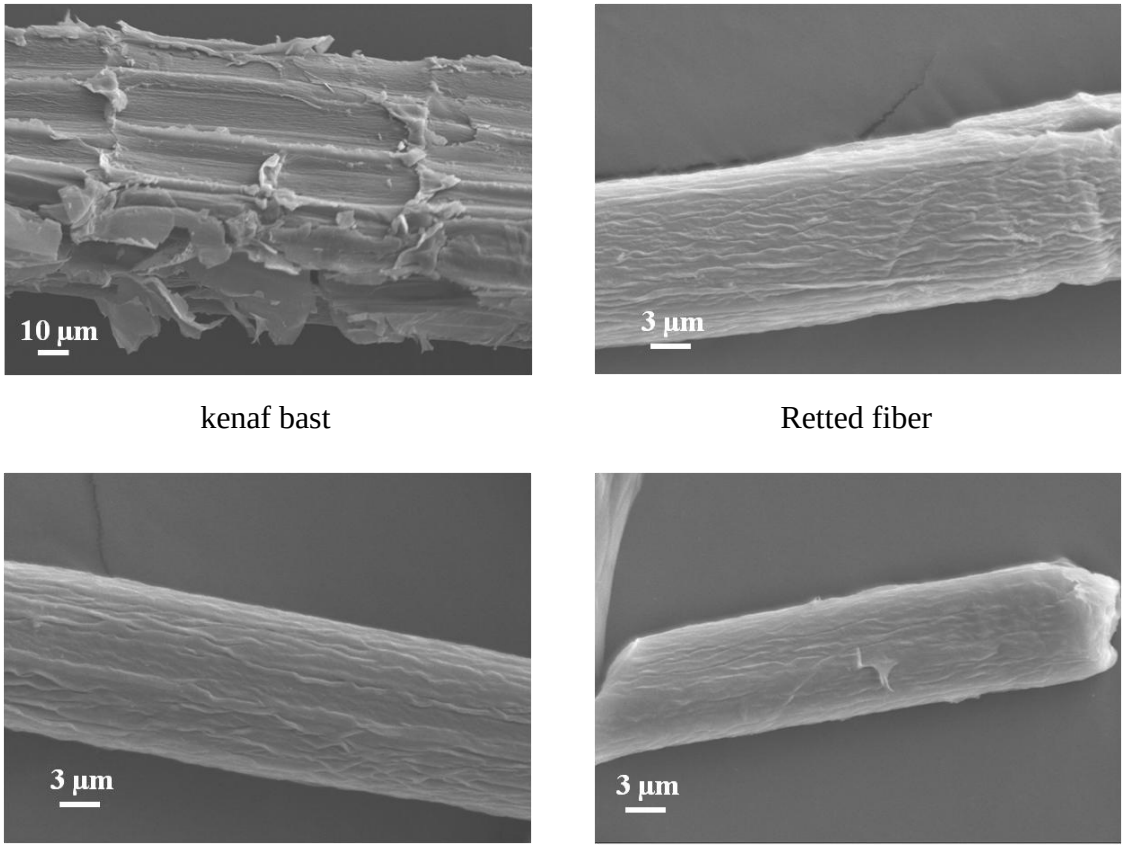

kenaf bast Retted fiber

Bleached fiber Microfiber

Figure 4.2 SEM images of kenaf bast, retted fiber, bleached fiber and microfiber.

The raw kenaf bast fiber had a rougher surface and larger diameter than the retted fiber and the bleached fiber. Through the alkaline retting process, small fibers were liberated from the kenaf bast fiber bundles. The bleached fiber morphology was altered little by the bleaching compared to that of retted fibers. Microfibers had a shorter length

than retted fibers and bleached fibers because of the cleavage of cellulose molecular chain at the amorphous regions.

CNWs images are shown in Figure 4.3.

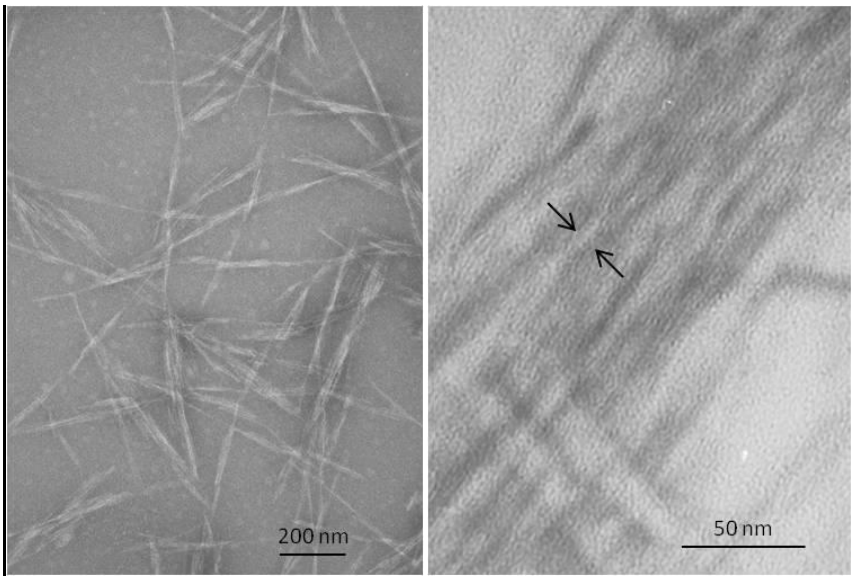

(a) 50,000X (b) 370,000X

Figure 4.3 TEM images of CNWs. The labels mean the magnifications.

The lengths of the CNWs were in a range from 100 to 1400 nm, and the diameters ranged from 7 to 84 nm. The aspect ratios ranged from 5 to 450, with an average value of 19.5. In some related research, CNWs had different dimensions. For instance, Roohani (2008) reported the average length and width were about 172 nm and 15 nm respectively, leading to an average aspect ratio of around 11 to 12. The diameter of the needle-like microcrystalline cellulose prepared by Lee (2009) was around 100 nm. The cellulose nanofibers prepared from flax fiber (Qua 2009) showed a diameter of around 9 nm, a length of around 141 nm, and an average aspect ratio of 16.6. The differences in

fiber dimensions from different studies may be due to the different fiber resources and preparation methods.

Individual CNWs were composed of several parallel aligned cellulose crystallites. These can be observed in Figure 4.3 (b) between the two arrows. The width of a crystallite is about 5.4 nm. The dimensions of the monoclinic unit cell of the regenerated cellulose were reported as a = 0.814 nm, b = 0.919 nm, and c = 1.03 nm (fiber axis) (Nugmanov *et al*. 1987). The widths of the CNWs were in a range from 7 to 84 nm, while the lengths were 100-1400 nm. Therefore, individual CNWs obtained in this study were composed of 100 to 1300 unit cells aligned in the direction of the fiber axis (c). A cross section of an individual CNW consisted of eight to 103 unit cells, or, one to 15 crystallites.

4.3.3 Fiber dimension analysis

The mean value and standard deviation of the length and diameter are shown in Table 4.1.

Table 4.1 Dimensions of the hierarchical fibers.

		Retted fibers (μm)	Bleached fibers (μm)	Microfibers (μm)	CNWs (nm)
Length	Mean	471.0	215.32	46.39	628.38
	Stdev.	606.98	141.62	16.38	360.05
	LSD Test	A	B	C	D
Diameter	Mean	10.70	10.63	9.58	34.75
	Stdev.	2.68	2.05	2.25	21.43
	LSD Test	A	A	B	C
Aspect ratio*	Mean	44.0	20.3	4.84	18.8

*Aspect ratios were calculated based on the ratio of the mean diameter to the mean length.

LSD tests indicated the fiber length was reduced significantly at each stage of the processes. However, each fiber had large length variations. The average diameter of bleached fibers was not significantly different than that of the retted fibers. The microfibers' diameters were significantly smaller than those of bleached fibers. The diameters of CNWs reached tens of nanometers, significantly smaller than microfiber diameters. Bleached fiber and CNWs had a higher aspect ratio than retted fiber and microfibers. Microfiber had the smallest aspect ratio.

4.3.4 Fourier Transform Infrared spectroscopy

In Figure 4.4, the Fourier Transform Infrared (FT-IR) spectra show the functional groups on the fiber surfaces, and within detectable regions below the fiber surfaces. Hydroxyl stretching vibrations are found between 3000 cm^{-1} and 3500 cm^{-1}. Clearly, a highly hydrogen bonded network exists, as indicated by the lower frequencies, with some free hydroxyls at high frequencies. The intensity of this peak envelope increased gradually, going from untreated fiber, retted fiber, bleached fiber, microfiber, to nanofiber because the specific surface area of the fibers increased. More hydroxyl groups in the surface and in the detectable regions below the surface are exposed as the fiber size is reduced from the micron scale to the nanometer scales. The peaks at 2896.6 cm^{-1}, 1718.3 cm^{-1}, 1307.5cm^{-1}, and 1020 cm^{-1} represent the C-H, C=O, C-O, and C-C stretching, respectively. The peak at 1648.8 cm^{-1} (C=C stretching), found in untreated kenaf bast fibers, disappeared in all the treated fibers. This corresponds to the removal of carbon-carbon unsaturation present in lignin components and extractives.

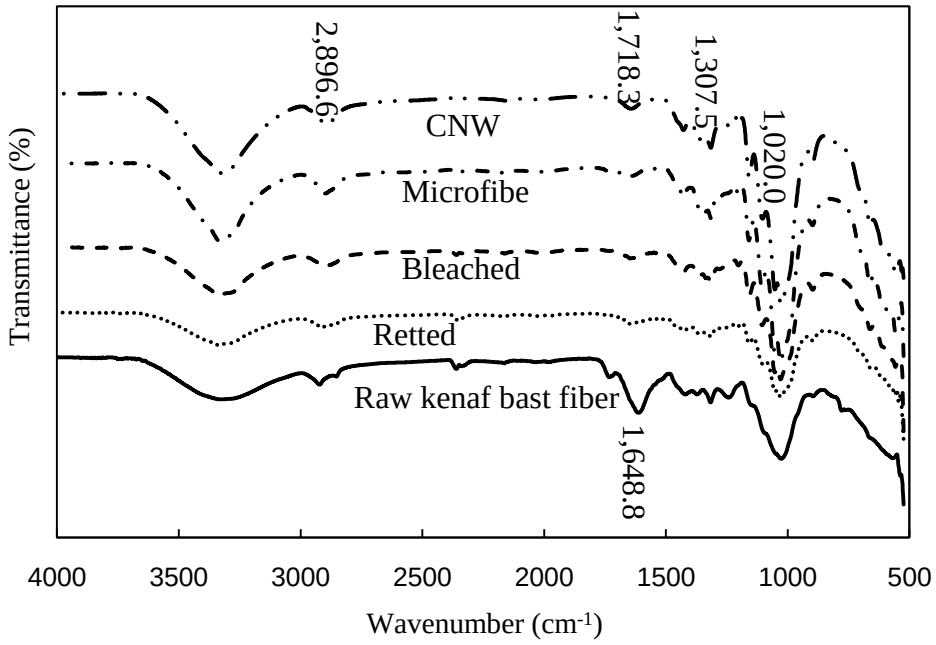

Figure 4.4 FT-IR spectra of the hierarchical fibers.

4.3.5 Fiber crystallinity

The X-ray diffraction spectra of the fibers are shown in Figure 4.5. The calculated degrees of crystallinity of the fibers are shown in Figure 4.6. The fiber crystallinity gradually increased at each stage of the process. Alkaline retting removed lignin and hemicelluloses, so the crystalline regions of cellulose took up a higher percentage in a whole fiber. Bleaching with hydrogen peroxide accelerated the cleavage of the cellulose molecular chains within the amorphous regions, resulting in a further increase of the crystallinity.

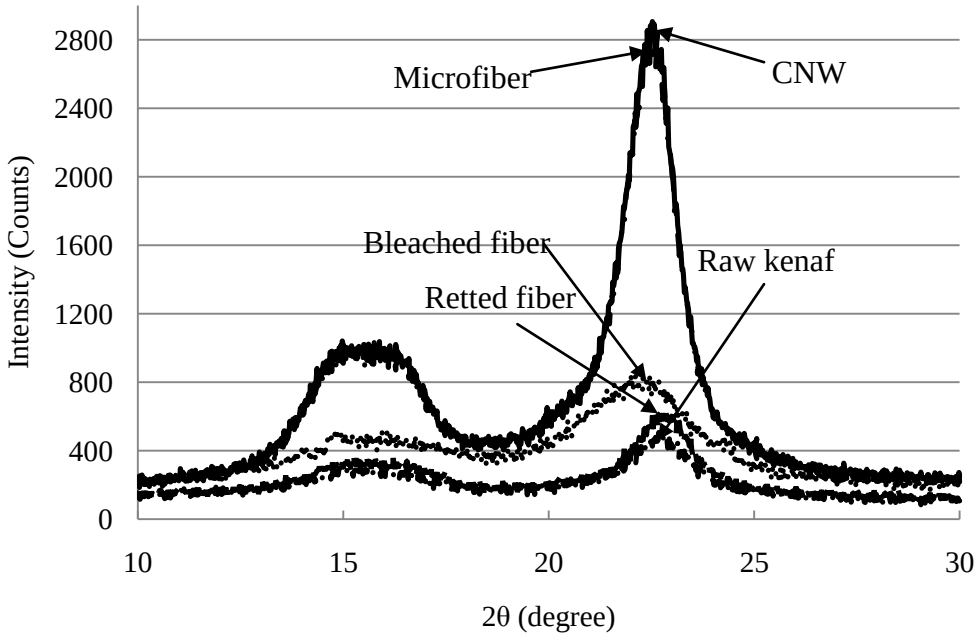

Figure 4.5 X-ray diffraction spectra of the hierarchical fibers.

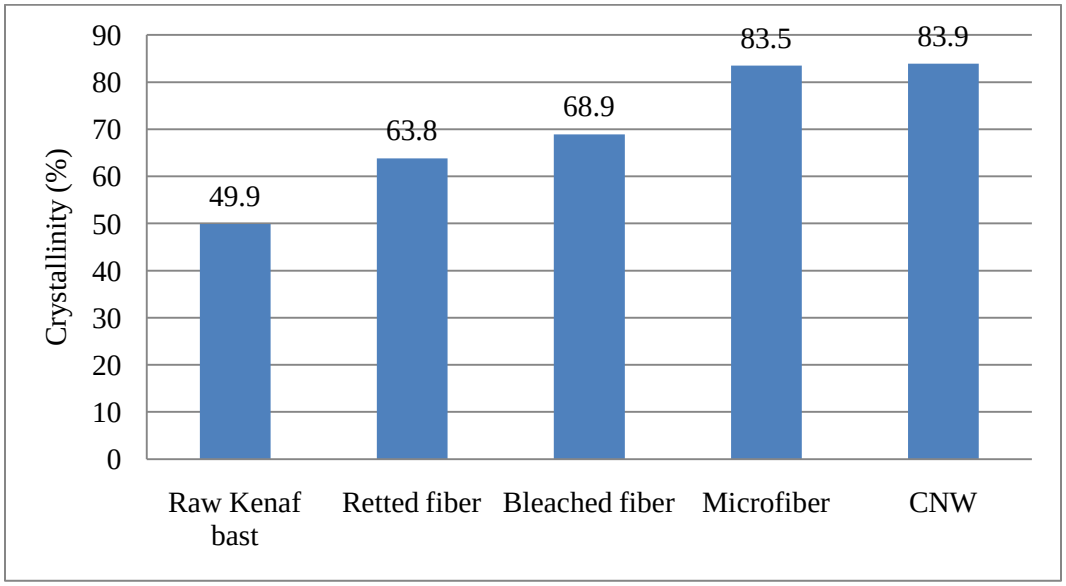

Figure 4.6 Crystallinities of the hierarchical fibers.

Acid hydrolysis improved the crystallinity of the fibers significantly by the cleavage of glycosidic bonds in cellulose molecular chains within amorphous regions. Amorphous regions were greatly diminished, while crystalline regions were highly resistant to acid hydrolysis. Therefore, microfibers and CNWs have the highest crystallinity among the fibers.

4.4 Conclusions

Pure cellulose fibers from the micron scale to the nanometer scale were obtained. Approximately 22.6% of the α-cellulose in kenaf bast could be converted into CNWs. The fiber crystallinity increased at each stage of the chemical processes. A high crystallinity of CNW, about 84%, was obtained.

CHAPTER V

POLYMER COMPOSITES REINFORCED WITH KENAF BAST FIBERS

5.1 Materials

Composites were made from three types of fibers: 1) kenaf fibers retted with the hermetical alkaline retting process described in Chapter II; 2) INI-treated kenaf fibers prepared with the INI treatments described in Chapter III, and 3) the CNWs prepared with the chemical processes described in Chapter IV.

Polypropylene film (PP: CO-EX Oriented Polypropylene), provided by Plastic Suppliers, Inc. Dallas, TX, was used to fabricate composites with retted fibers and INI-treated fibers. Polyvinyl alcohol (PVA) (MW=100,000) powder (Fisher Scientific) was used to fabricate the composites with CNWs.

5.2 Methods

5.2.1 Fabrication of kenaf fiber/PP composites

Polyprolylene (PP) was applied as a matrix. The retted kenaf fibers and INI-treated fibers were used as reinforcements respectively. The composites were fabricated with a sheet molding compound process. The retted kenaf fibers and INI-treated kenaf fibers were dispersed in water by vigorous mechanical stirring. The fiber suspension was

poured into a 355 mm × 355 mm deckle box and then passed through a screen (mesh 35), on which the fiber sheets were formed as the water flowed down gravitationally. The fiber sheets were dried in an oven set at 80 ℃. The fiber sheets and PP films were cut into a dimension of 15.2 cm × 15.2 cm and laminated alternatively. The fiber to PP weight ratio in the composite panel was 50: 50. The laminated mats were pressed at 200 ℃ and 0.7 MPa for 2.5 minutes. The pressure was not released until the platen was cooled to room temperature. The laminated kenaf fiber/PP panels were removed from the press and stored in a desiccator with silica gel for two days before preparing the mechanical testing specimens. Three panels were fabricated for each formula. The density of all the kenaf fiber/PP composites (including the retted kenaf fibers reinforced and INI-treated kenaf fibers reinforced composites) was 0.88 ± 0.03 g/cm^3.

5.2.2 Fabrication of CNW/PVA composites

CNW/PVA composites were fabricated with a film casting process. PVA aqueous solutions were mixed with CNW aqueous suspensions followed by ultrasonic treatment for 5 min (750 watts, 20 kHz, 40% amplitude of vibration) to homogenize the distribution of CNWs in the matrix. The weight ratios of CNW to PVA were 1:99, 3:97, 6:94 and 9:91, respectively. CNW/PVA composite films, with the CNWs loading of 1 wt%, 3 wt%, 6 wt% and 9 wt%, were fabricated after the water evaporated. CNW/PVA composites were dried at 50 ℃ for 12 hours and stored in vacuum bags before analysis and testing.

5.2.3 Dimensional analysis of CNWs

CNW specimens for TEM analysis were prepared by dropping the water suspension of CNWs on a carbon coated microscope grid followed by drying for approximately 15 minutes. To study the morphology of the CNW/PVA composites, a reformed method was applied to prepare the specimens, since the conventional microtome method was not feasible for CNW/PVA composites because of the water solubility of PVA. The reformed technology started with the dissolution of the CNW/PVA composites in distilled water, followed by loading the composites water solution on the carbon coated microscope grids then drying for about 30 min. Hence, a thin layer of CNW/PVA composites was formed on the grid. The specimens were stained with 2% uranyl acetate before microscope analysis. The morphology of pure CNWs and the CNW/PVA composites were studied with TEM (JEOL-100CX II Electron Microscope) at an accelerating voltage of 80kV. Fifty CNWs were randomly measured for their lengths and diameters from the CNW/PVA composite containing 9 % CNWs.

5.2.4 Composites tensile properties testing

Tensile properties of the INI-treated kenaf fiber/PP composites, retted kenaf fiber/PP composites, and CNW/PVA composites were tested with Instron 5869 (load cell 50kN). The crosshead extensions were used as the specimen deformations. Composites samples were kept in desiccators for one week before tensile testing. The procedures referred to ASTM 1037. Cross-head speed during tension testing was 2.5 mm/min for kenaf fiber/PP composites, and 50 mm/min for CNW/PVA composites. The reason for using two different loading speeds for the composites is that kenaf fiber/PP composites have a much lower elongation than CNW/PVA composites. Nine replicates of each

composite formulation were tested. Multiple comparison of the results were conducted with Fisher's Least Square method at α=0.05 using SAS 9.2 software (SAS Institute Inc. NC, USA). The fracture surfaces of the samples were observed using scanning electron microscopy (SEM, Zeiss Supra TM 40).

5.2.5 Thermal properties analysis

A differential scanning calorimeter (DSC, Setaram Instrumentation, DSC 131) was used to analyzed the thermal behavior of the composites. The tests were performed from room temperature (23 ℃) to 200 ℃ with a nitrogen atmosphere. The flow rate of the nitrogen was 100 mL/min. The heating rate was 10 ℃/min from room temperature to 200 ℃ followed by the constant temperature of 200 ℃ for 10 min. Subsequently, temperature dropped to 23 ℃ at a rate of 3 ℃/min. An empty pan was used as the reference. The composite samples were weighted to exactly 11.7 mg. The initial crystallinity of PP matrix can be determined by comparing the melting enthalpy to the value of 100% crystalline sample using equation 5-1 (Lee *et al*. 2007). The melting enthalpy of the sample can be obtained from the endothermic curve. As the molten PP cools to room temperature, an exothermic curve can be obtained. The crystallization enthalpy can be derived from the curve. The final crystallinity of PP can be calculated using equation 5-1 also.

$$X_c = \left(\frac{\Delta H_f}{m\,\Delta H_{f100\%}}\right) \times 100\% \qquad (5\text{-}1)$$

where: X_c = the crystallinity of PP, %;

ΔH_f = the heat of fusion, mJ;

m = the mass of PP, mg;

$\Delta H_{f100\%}$ = the melting enthalpy of 100% crystalline PP, J/g.

$\Delta H_{f100\%}$ cannot be obtained directly in experiments but is calculated from the structural data of the crystallites determined using X-ray diffraction. $\Delta H_{f100\%}$ of PP is known from literature (Schubnell 2001) as 207 J/g.

5.3 Results and discussion

5.3.1 Kenaf fiber/PP composites

5.3.1.1 Tensile properties of the retted kenaf fiber/PP composites

The results of tensile moduli and tensile strengths of the retted kenaf fiber/PP composites are shown in Figure 5.1 and 5.2.

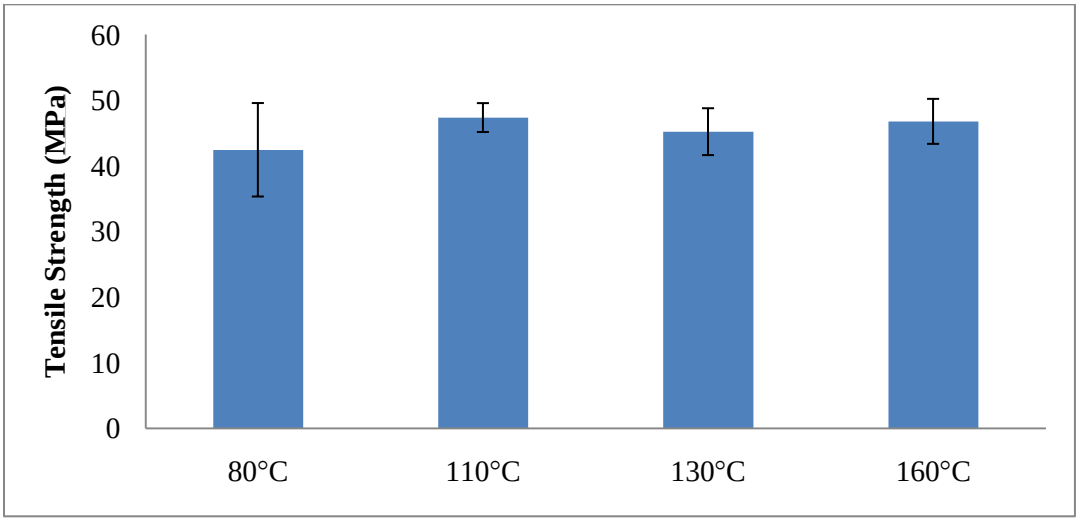

Figure 5.1 Tensile strength of retted kenaf fiber/PP composites.

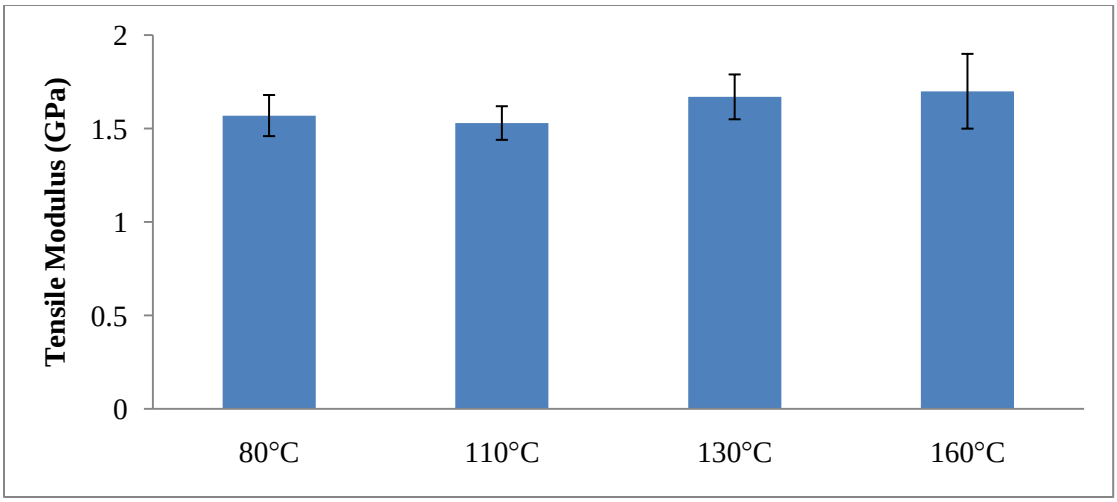

Figure 5.2 Tensile moduli of the retted kenaf fiber/PP composites.

Statistical analysis indicated there was no significant difference in the tensile moduli and tensile strengths at the 95% significance level among the four types of composites.

The typical stress-strain curves of the retted kenaf fiber/PP composites are shown in Figure 5.3.

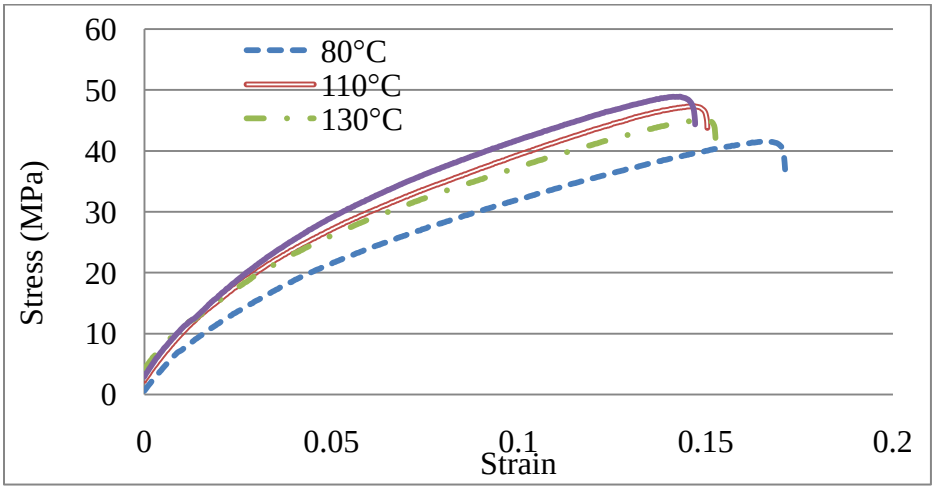

Figure 5.3 Stress-strain curves of the retted kenaf fiber/PP composites.

The non-linearity of the curves is due to the plastic deformation of the composites. Kenaf fibers are readily dislocated because of the poor interfacial adhesion between kenaf fibers and PP matrix. Therefore, the stress-strain curves suggest plastic deformation.

The fracture surface SEM images are shown in Figure 5.4. Generally, the fracture surface images indicated the compatibility between the retted fibers and PP matrix was poor, as evidenced by the complete separation between the fibers and PP matrix. Therefore, surface modification for the retted fibers is necessary to improve the compatibility between the fibers and the PP matrix.

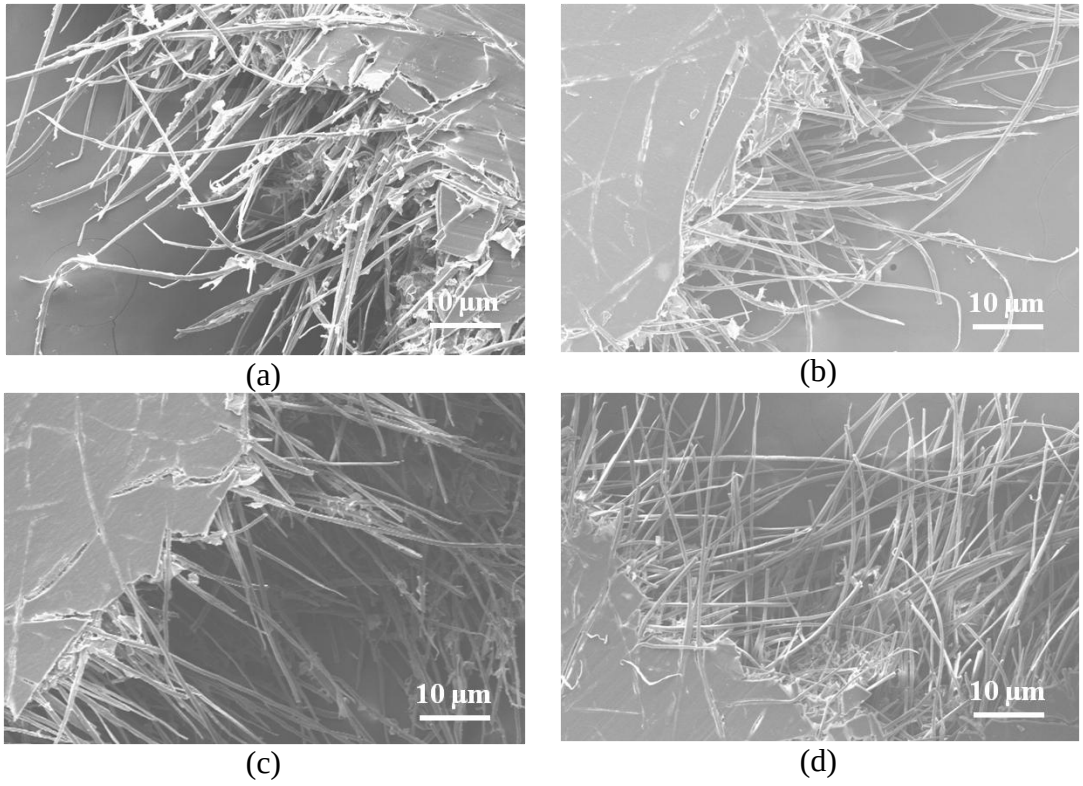

Figure 5.4 Fracture surface SEM images of the retted kenaf fiber/PP composites. The kenaf fibers were retted at (a) 80 ℃, (b) 110 ℃, (c) 130 ℃ and (d) 160 ℃.

5.3.1.2 Tensile properties of the INI-treated kenaf fiber/PP composites

The tensile strengths and tensile moduli of INI-treated kenaf fiber/PP composites are shown in Figure 5.5 and 5.6.

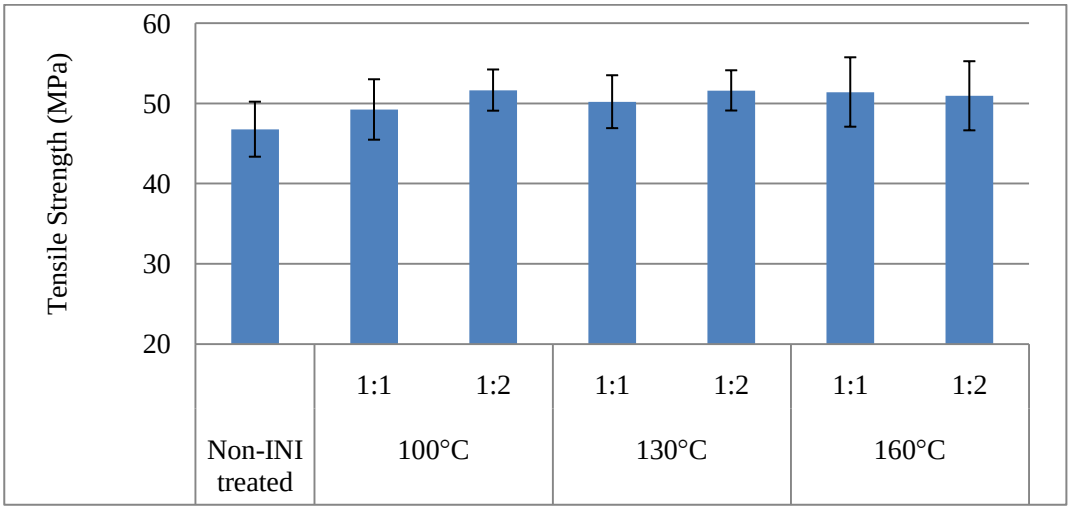

Figure 5.5 Tensile strengths of INI-treated kenaf fiber/PP composites. The labels mean the INI treatments conditions for the kenaf fibers. Non-INI treated fiber is the fibers retted at 160°C but not treated with INI processes.

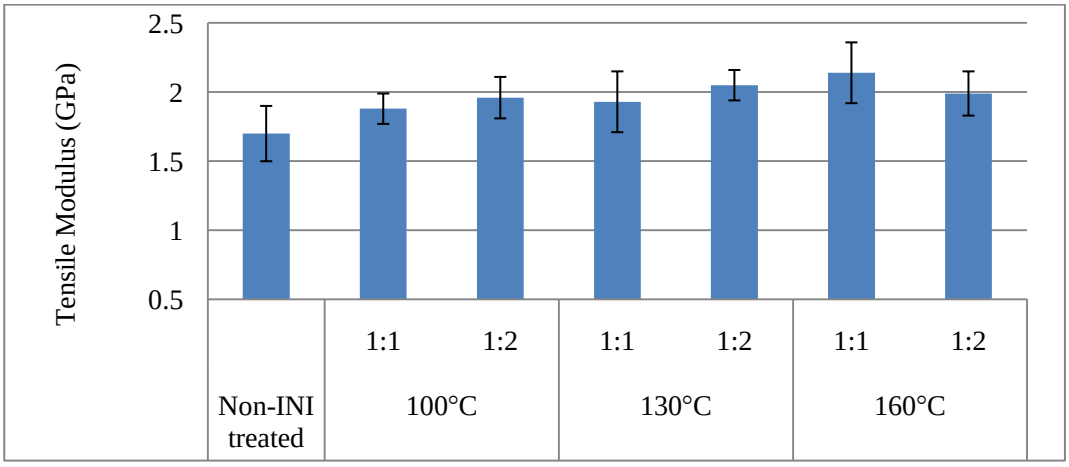

Figure 5.6 Tensile moduli of INI-treated kenaf Fiber/PP composites. The labels mean the INI treatments conditions for the kenaf fibers. Non-INI treated fiber is the fibers retted at 160°C but not treated with INI processes.

Except for the composites reinforced with the fibers retted at 100 ℃ (Na_2CO_3 : $CaCl_2$ =1:1, mol:mol), the tensile strengths of the composites reinforced with INI-treated kenaf fibers were significantly higher than that of the composites reinforced with non-INI-treated fibers. No significant difference in tensile strengths was found among the six INI treatment conditions.

All the INI-treated fibers significantly improved the composites tensile moduli compared to that of the composites reinforced with non-INI-treated fibers. The composites reinforced with the INI-treated fibers, whose treatment condition was 160 ℃ (Na_2CO_3 : $CaCl_2$ =1:1, mol:mol), yielded the highest tensile modulus, 25.9% higher than that of the composites reinforced with non-INI-treated fibers.

The typical stress-strain curves of the INI-treated kenaf fiber/PP composites are shown in Figure 5.7.

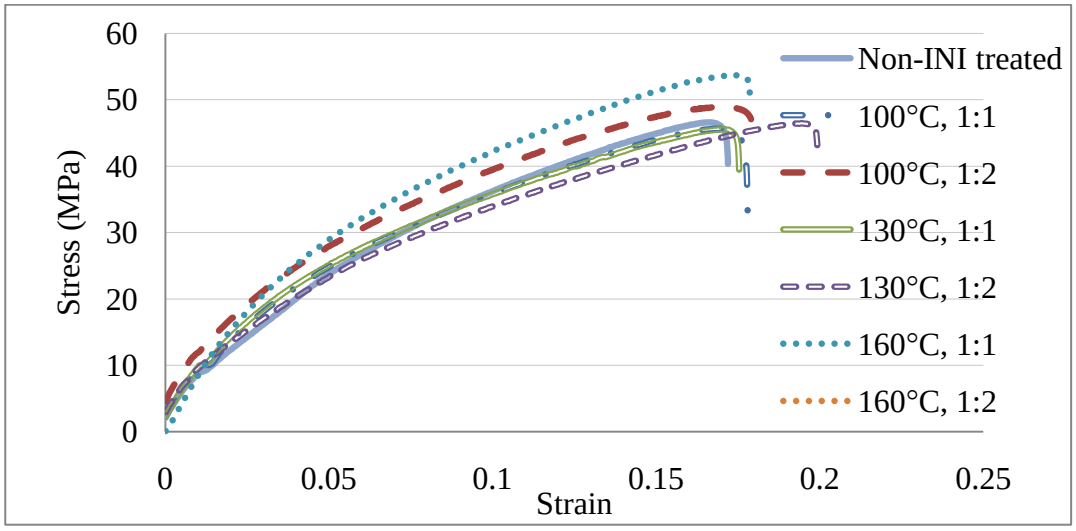

Figure 5.7 Stress-strain curves of the INI-treated fiber/PP composites. The labels mean the INI treatments conditions for the kenaf fibers. Non-INI treated fiber is the fibers retted at 160°C but not treated with INI processes.

Since the load taken up by the fibers decreases as the strain increases (Rowell *et al*. 1999), the tensile behaviors of the composites drive toward plastic deformation and the slopes of the stress-strain curves become smaller as the strain increases. The dislocation of INI-treated kenaf fibers in the composites may occur under a higher load than non-INI-treated fibers because $CaCO_3$ particles modified the compatibility between kenaf fiber and PP matrix. The initial slopes of the stress-strain curves are higher for INI-treated kenaf fiber/PP composites than that for non-INI treated kenaf fiber/PP composites.

Figure 5.8 shows the SEM images of the fracture surfaces of the INI-treated kenaf fiber/PP composites and the control composite.

The control composite was PP composites reinforced with kenaf fibers retted at 160°C but not treated with INI processes. Fiber pull-out is clearly shown at the fracture surface of the non-INI-treated fiber/PP composites (Figure 5.8, Non-INI-treated), indicating a poor fiber-PP interfacial compatibility. Simultaneous failures of INI-treated kenaf fiber and PP matrix occurred in the INI-treated fiber/PP composites (Figure 5.11, 130°C, 1:1 and 160°C, 1:2). The strong adhesion between INI-treated kenaf fibers and PP matrix resulted in the difficulty of the dislocation between the fibers and PP matrix (Figure 5.11, 100°C, 1:1). These results evidenced that the compatibility between kenaf fiber and PP matrix was modified by the $CaCO_3$ particles loaded in the kenaf fibers by the INI treatments.

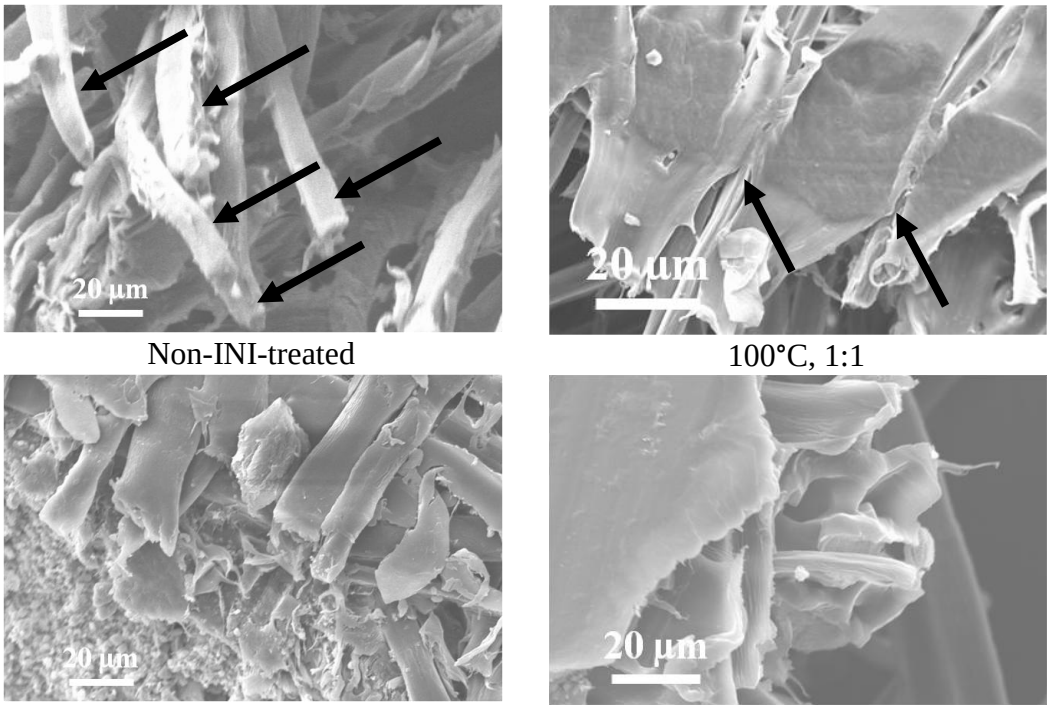

Non-INI-treated | 100°C, 1:1 | 130°C, 1:1 | 160°C, 1:2

Figure 5.8 SEM images of the fractural surfaces of INI-treated kenaf fiber/PP composites. The labels mean the reaction temperatures and the molar ratios of Na_2CO_3 to $CaCl_2$. Non-INI treated fiber is the fibers retted at 160°C but not treated with INI processes.

5.3.1.3 Thermal properties of the kenaf fiber/PP composites

The enthalpies, onset temperatures, and peak temperatures of melting and crystallization of pure PP, the retted kenaf fiber/PP composite, and the INI-treated kenaf fiber/PP composite were obtained by DSC analysis and were quantitatively shown in Table 5.1.

In the endothermic behavior, the melting process of PP initiated at 126.8℃ in the retted kenaf fiber/PP composite and 129.7°C in INI-treated kenaf fiber/PP composite, earlier than that of pure PP (153.0°C). The peak melting temperatures of PP in the two composites slightly decreased compared with that of pure PP. The decreases in the onset

melting temperature can be interpreted by the formation of crystalline defects or small crystals of PP in the composites. The factors causing the melting temperature reduction include the finite size of the crystallites, their state of internal perfection, and the interfacial and connecting regions (Nadkarni *et al*. 1991; Mago *et al*. 2009). Kenaf fibers provided more nucleation sites for PP, so the crystallization of PP could initiate at a number of nucleation sites with finite rates. The deviations from equilibrium resulted in the lower onset melting temperatures.

Table 5.1 Thermal characteristics of the kenaf fiber/PP composites and pure PP.

		Pure PP	Retted fiber/PP	INI-treated fiber/PP
Endothermic behavior	T_o (°C)	153.00	126.77	129.70
	T_m (°C)	166.30	162.89	163.72
	ΔH (J/g)	62.40	74.30	77.09
	X_c (%)	30.15	35.89	37.24
Exothermic behavior	T_o (°C)	122.30	142.20	144.20
	T_c (°C)	116.90	132.10	133.90
	ΔH (J/g)	64.95	84.64	81.35
	X_c (%)	31.38	40.89	39.30

T_o is onset temperature. T_m is peak melting temperature. T_c is peak crystallization temperature. ΔH is enthalpy. X_c is crystallinity. Retted fiber/PP is the PP composite reinforced with the kenaf fibers that were retted at 160C but not INI-treated. INI-treated fiber/PP is the PP composite reinforced with the kenaf fibers that were INI-treated at 160°C (Na_2CO_3: $CaCl_2$ = 1:1, mol: mol).

The melting enthalpies of PP in the two composites were both higher than that of pure PP. This can be explained by their higher crystallinities. The more crystalline regions it has, the more energy it requires to liberate the molecular chain from the crystalline structure.

In the exthothermic behavior, the crystallization of PP initiated earlier in the composites than that in pure PP. The peak crystallization temperatures of PP in the composites were about 20°C higher than that of pure PP. This may be because the fiber surface provided nucleation sites for PP. The formation of a higher crystalline PP structure needs more energy. This is the reason for the higher enthalpies in the composites than that in pure PP. Because of the nucleation sites, the crystallinility of PP in the composites was higher than that of pure PP. This conclusion agrees with Lee's studies (Lee *et al*. 2010, 2007).

There is little difference in the thermal characteristics between retted kenaf fiber/PP composites and INI-treated kenaf fiber/PP composites.

5.3.2 CNW/PVA composites

5.3.2.1 Distributions of CNWs dimensions in CNW/PVA composites

The TEM images of the CNWs in the CNW/PVA composites are shown in Figure 5.9. The lengths and diameters distributions of the CNWs before and after incorporation in the CNW/PVA composite containing 9 % CNWs are shown in Figure 5.10. Agglomeration of the CNWs tended to form as CNWs weight ratio increased. The agglomeration of CNWs was also suggested by the distributions of CNWs lengths and diameters in the composites compared with those of pure CNWs (Figure 5.10). However, the LSD test (Table 5.2) suggested that CNWs diameters and lengths in composites were not changed significantly by agglomeration.

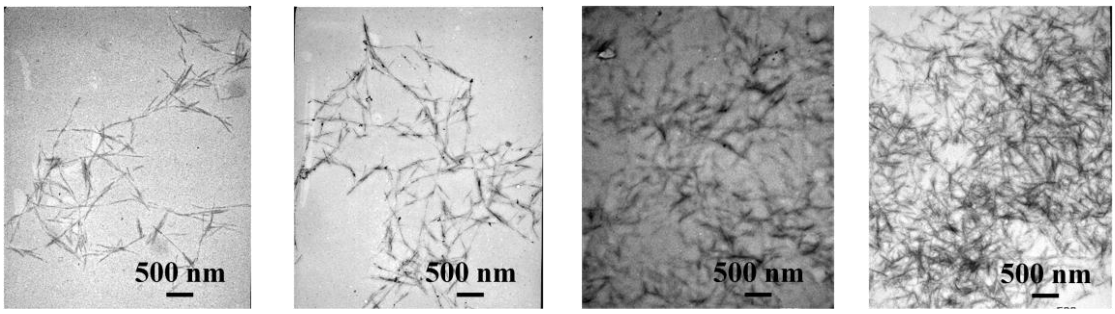

(a) (b) (c) (d)

Figure 5.9 TEM images of CNW/PVA composites. Magnification = 14,000X. (a) Weight ratio of CNW=1%; (b) Weight ratio of CNW=3%; (c) Weight ratio of CNW=6%; (d) Weight ratio of CNW=9%.

Table 5.2 Lengths and diameters of CNWs in the CNW/PVA composite.

		CNW (nm)	CNW in composites*(nm)
Length	Mean	628.38	662.62
	Standard deviation	360.05	249.04
	LSD test	A	A
Diameter	Mean	34.75	40.63
	Standard deviation	21.43	13.79
	LSD test	A	A

*The composite contains 9 % CNWs.

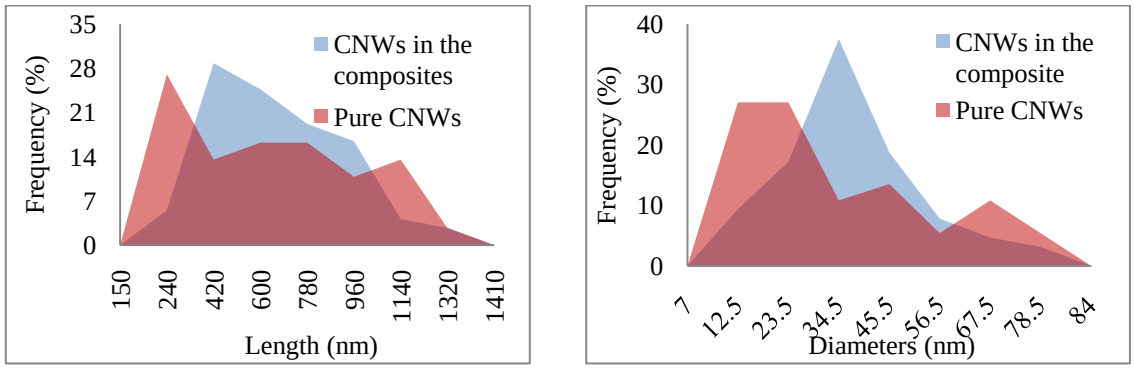

Figure 5.10 Length and diameter distributions of CNWs before and after incorporation in the CNW/PVA composite. The CNW/PVA composite contains 9 % CNWs.

5.3.2.2 Tensile properties of CNW/PVA composites

The tensile strengths and tensile moduli of the CNW/PVA composites are shown in Figure 5.11 and 5.12. Statistical analysis showed the average tensile strength of the CNW/PVA composites fabricated with 3 % CNW and 9 % CNWs were significantly different, and the tensile strength of the CNW/PVA composites fabricated with 3% CNWs was significantly different from that of pure PVA. The tensile strength of the composite increased by 24.2% when 3 % CNWs were incorporated in the composite and increased by 46.4% when 9% CNW was employed. Tensile modulus of the composite with 3 % and 6 % CNWs were improved by 63.27% and 66.18% respectively compared with pure PVA. Nine percentage CNWs improved the tensile modulus by 152.3% and 51.82% compared with pure PVA and the composites with 6 % CNWs respectively.

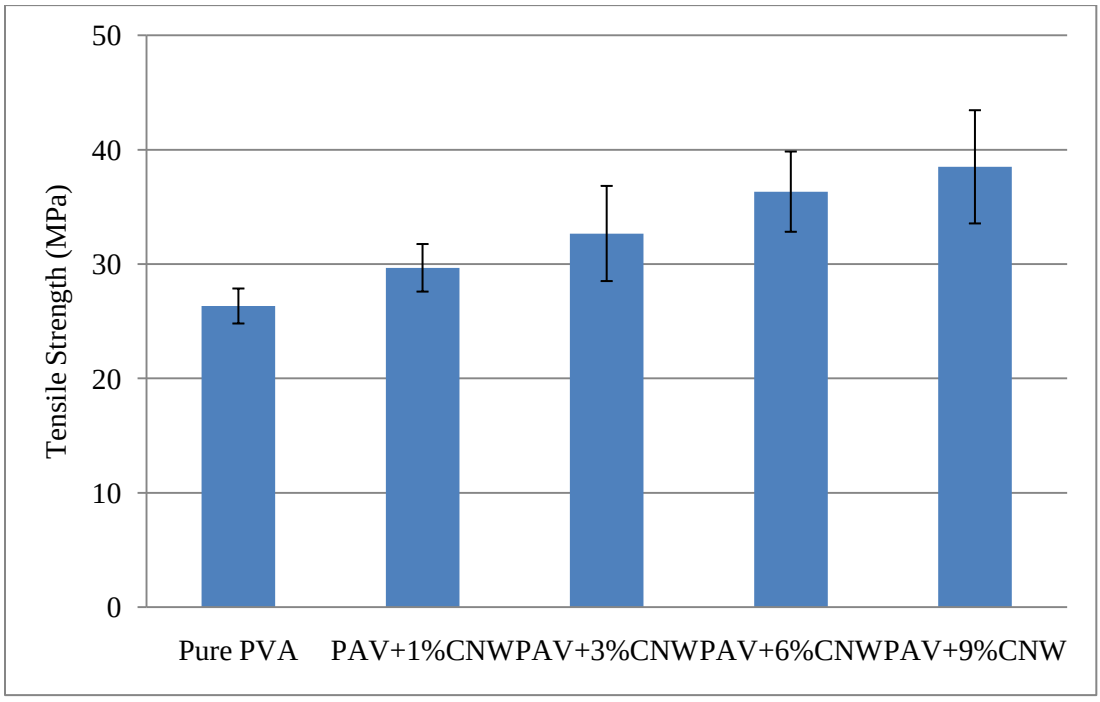

Figure 5.11 Tensile strengths of the CNW/PVA composites.

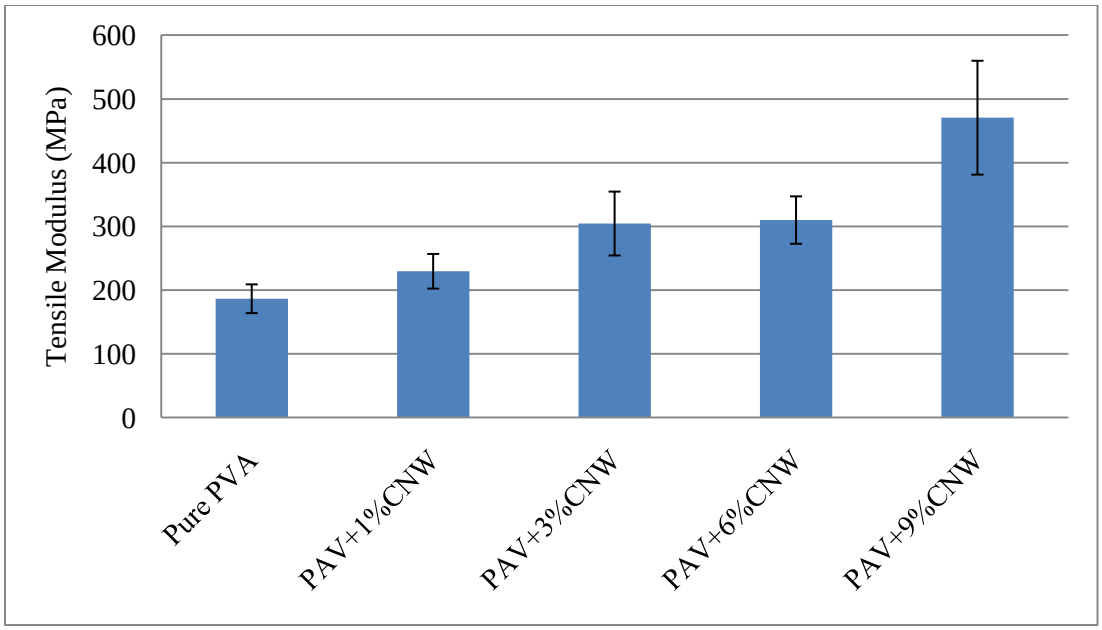

Figure 5.12 Tensile moduli of the CNW/PVA composites.

Bhatnagar (2005) indicated that the cellulose nanofibers prepared from different fibers, such as hemp, rutabaga, flax, and kraft pulp, would yield different reinforcements. The CNWs prepared form kenaf bast fiber in this study had a greater contribution to the tensile strength of the PVA composites than those from flax bast fiber in Bhatnagar's (2005) study (10.2% improvement with 10 wt.% cellulose nanofiber addition in PVA composites). However, the CNWs from kenaf bast fiber provided less reinforcement than those from rutabaga and hemp. Lee (2009) reported 1 wt.% loading of nanocellulose resulted in a significant increase of the tensile strength, but when the nanocellulose loading was increased to 3 and 5 wt.% to the PVA matrix, the tensile strengths gradually decreased. However, Qua (2009) showed that 5 wt.% microcrystalline cellulose addition in PVA composites only improved the tensile strength by 2%. The discrepancy in these

results may be due to the differences in the fiber characteristics, such as the aspect ratio, crystallinity, morphology, etc.

The typical stress-strain curves of the CNW/PVA composites are shown in Figure 5.13.

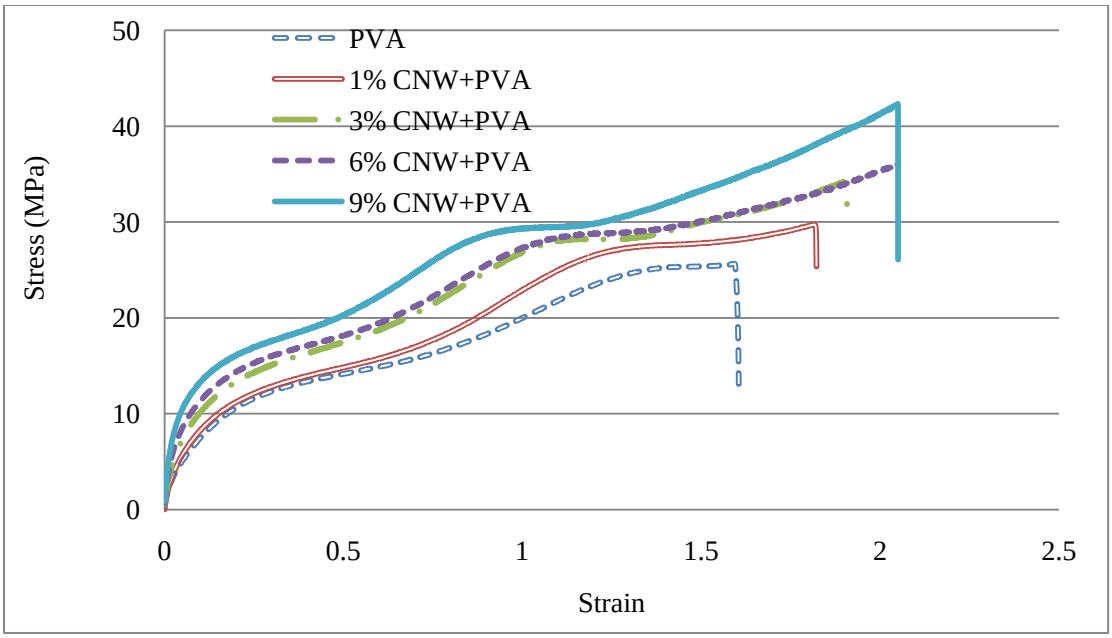

Figure 5.13 Stree-strain curves of the CNW/PVA composites.

The curves initiated with proportions of linearity and continued with non-linearity. The linear proportions indicate the elastic deformation of PVA matrix. The non-linear curves were due to the plastic deformation of PVA matrix. The unfolding of the PVA molecules in the amorphous regions caused the plastic deformation and large strain. As the weight percentages of CNWs increases in the composites, the slopes of the linear proportions increase, suggesting the tensile moduli increases. The train of the composites increases as the CNWs loading increases also, suggesting the elongations increase.

CNWs and PVA matrix have good compatibility because CNWs and PVA molecules both contain many hydroxyl groups. CNWs may hold the deformation of PVA molecules and transfer stress between the PVA molecules. Therefore, the CNW/PVA composites take higher stress than pure PVA to yield the same strain.

The SEM images of the fracture surface of the CNW/PVA composites are shown in Figure 5.14.

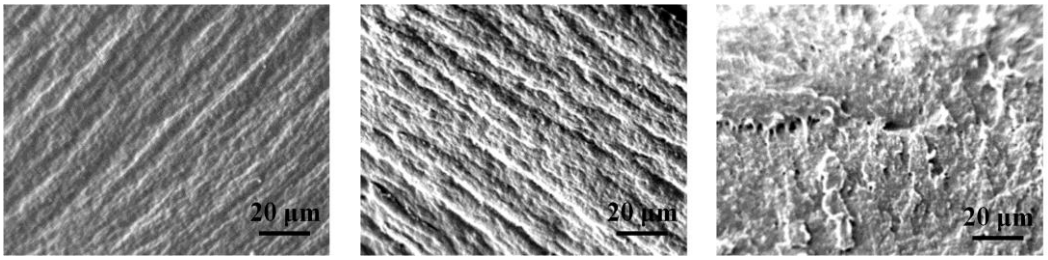

(a) (b) (c)

Figure 5.14 SEM Images of fracture surfaces of CNW/PVA composites. (a) pure PVA; (b) CNW/PVA composites with 3% CNWs; (c) CNW/PVA composites with 9% CNWs.

The SEM images of the fracture surfaces suggested that cracks were formed in CNW/PVA composites before failure. Few cracks were generated in pure PVA, while the largest numbers of cracks were found in the CNW/PVA composites fabricated with 9% CNW. The cracks are consistent with high energy absorption. This is why the CNW/PVA composites (9% CNW) had the highest tensile strength. The cracks resulted from high interlaminar shear strength between CNW and PVA. The high interlaminar shear strength may be due to good surface compatibility between CNW and PVA.

5.4 Conclusions

The retted fibers not treated with INI treatments had poor compatibility with the PP matrix. The INI treatment improved the compatibility between the kenaf fibers and the PP matrix, resulting in an improvement in tensile modulus and tensile strength of the kenaf fiber/PP composites. The CNWs prepared from kenaf bast had excellent reinforcement effects for PVA. The CNW/PVA composite containing 9 % CNWs yielded a significant improvement in the tensile strength and the tensile modulus by about 46% and 152%, respectively, compared with pure PVA.

CHAPTER VI

SUMMARY AND FUTURE WORK

6.1 Summary

Individual cellulosic fibers were obtained from kenaf bast with the hermetical alkaline retting process. The retted fibers had uniform dimensions and were suitable for sheet molding compound process. Micropores were generated in the cell wall of the fibers retted at 130 ℃ and 160 ℃. The retted fibers had poor compatibility with the PP matrix. $CaCO_3$ particles were successfully synthesized in the retted fibers with inorganic nanoparticle impregnation (INI) treatments. The $CaCO_3$ crystals initiated in the micorpores and were finally exposed on the fiber surface. $CaCO_3$ particles improved the compatibility between kenaf fibers and the PP matrix, resulting in the improvements of the tensile strength and the tensile modulus of the kenaf fiber/PP composites. Approximately 23% of the α-cellulose in kenaf bast was converted to cellulose nanowhiskers (CNWs) with the chemical processes. The yield of CNWs was 10.4% based on the mass of the raw kenaf bast. The CNWs had excellent reinforcements for polyvinyl alcohol (PVA). The CNW/PVA composite that contained 9 % CNWs yielded a significantly improvement in the tensile strength and the tensile modulus—about 46% and 152% respectively compared with pure PVA.

6.2 Future work

More studies will be conducted based on this dissertation. They include the following: (1) The porosity of the retted fibers will be estimated and used to predict the fiber properties and $CaCO_3$ loading weight percentage. (2) The effects of the molar ratio of Na_2CO_3 to $CaCl_2$ on the formation of $CaCO_3$ crystals will be investigated. The size of $CaCO_3$ could be controlled with the molar ratios and the reaction temperatures. (3) The mechanism of the interaction between $CaCO_3$ and PP will be studied. (4) The INI treatment conditions will be optimized to obtain kenaf fiber/PP composites that have the best properties. (5) The application of CNWs will be expanded not only for hydrophilic polymers but also for hydrophobic polymers. (6) Alignment of CNWs will be achieved with magnetic fields. The polymer composites reinforced with CNWs could be visibly transparent. The transparent composites with orientation-controlled CNWs will be fabricated.

REFERENCES

Albersheim P, Darvill A, Roberts K, Sederoff, Staehelin A (2010) Plant cell walls. Garland Science Publishing, Oxford, UK. 228-229 pp.

Alemdar A, Sain M (2008) Biocomposites from wheat straw nanofibers: morphology, thermal and mechanical properties. Compos Sci Tech 68 (2): 557-565.

Alemdar A, Sain M (2008) Isolation and characterization of nanofibers from agricultural residues-wheat straw and soy hulls. Bioresource Tech 99 (6): 1664-1671.

Allan GG, Carroll JP, Negri AR, Raghuraman M, Ritzenthaler P, Yahiaoui A (1992) The microporosity of pulp: the precipitation of inorganic fillers within the micropores of the cell wall. Tappi J 75(1):175-178.

Aziz SH, Ansell MP, Clarke SJ, Panteny SR (2005) Modified polyester resins for natural fibre composites. Compos Sci Tech 65(3-4): 525-535.

Berglund LA, Peijs T (2010) Cellulose biocomposites-from bulk moldings to nanostructured systems. MRS Bulletin 35:201-206.

Berresheim AJ, Müller M, Müllen K (1999) Polyphenylene nanostructures. Chem Rev 99(7) : 1747-1785.

Bhatnagar A, Sain M (2005) Processing of cellulose nanofiber-reinforced composites. J Reinforc Plast Compos 24 (12):1259-1268.

Bledzki AK, Sperber VE, Faruk O (2002) Natural and wood fibre reinforcement in polymers. Rapra Review Reports, Rapra Technology Ltd., Shawberry, Shrewsbury, Shropshire, UK. 13(8):144.

Bura R, Gustafson R (2010) Lecture PSE 476/Chem E 471: Pulping and bleaching. College of Foreest Resources, University of Washington. http://www.cfr.washington.edu/classes.pse.476/notes.htm (20 May 2011).

Chabannes M, Ruel K, Yoshinaga A, Chabbert B, Jauneau A, Joseleau JP, Boudet AM (2001). *In situ* analysis of lignins in transgenic tobacco reveals a differential impact of individual transformations on the spatial patterns of lignin deposition at the cellular and subcellular levels. The Plant J 28(3): 271-282.

Chakraborty A, Sain M, Kortschot M (2005) Cellulose microfibrils: a novel method of preparation using high shear refining and cryocrushing. Holzforschung 59(1):102-107.

Clemons C, Sanadi AR (2007) Instrumented impact testing of kenaf fiber reinforced polypropylene composites: effects of temperature and composition. J Reinforc Plast Compos 26(15): 1587-1602.

Clemons CM (2005) Natural fibers. Pages 213-222 *in* M Xanthos, eds. Functional fillers for plastics. Wiley-VCH. Weinheim, Germany.

Clowes FAL, Juniper BE (1968) Plant cells. Blackwell Scientific Publications Ltd, Oxford, UK. 203-297 pp.

Eichhorn SJ, Baillie CA, Zafeiropoulos N, Mwaikambo LY, Ansell MP, Dufresne A, Entwistle KM, Herrera-Franco PJ, Escamilla GC, Groom LH, Hughes M, Hill C, Rials TG, Wild PM (2001) Review current international research into cellulosic fibres and composites. J Mater Sci 36 (9):2107-2131.

German Association of Cellulose Chemists and Engineers (1951) Bestimmung der alphacellulose und de langeunloslichen anteils von zellstoffen. Markblatt IV/29 Zellcheming.

Gindl W, Keckes J (2005) All-cellulose nanocomposite. Polymer 46 (23): 10221-10225.

Gordon JL (1969) Thermal decomposition of calcium carbonate. Master thesis, Texas Technological College, Lubbock, TX. 34-44 pp.

Green JW, Pearl IA, Haigh FC (1977) Fast reactions in alkaline pulping II: The peeling reaction. IPC Technical Paper Series, No. 42. The Institute of Paper Chemistry. Appleton, WI.

Henriksson M, Henriksson G, Berglund LA, Lindström T (2007) An environmentally friendly method for enzyme-assisted preparation of microfibrillated cellulose (MFC) nanofibers. Eur Polymer J 43(8): 3434-3441.

Hocking MB, Ong JH (1977) Kinetic studies of dakin oxidation of o- and p-hydroxyacetophenones. Can J Chem 55(1):102-110.

Hocking MB, Crow JP (1994) On the mechanism of alkaline hydrogen peroxide oxidation of the lignin model p-hydroxyacetophenone. Can J Chem 72(4): 1137-1142.

Holbery J, Houston D (2006) Natural-fiber-reinforced polymer composites in automotive applications. JOM 58(11): 80-86.

Holmgren A (2008) Biochemical control aspects in lignin polymerization. Doctoral thesis. Royal Institute of Technology, School of Chemical Sciences and Engineering, Department of Fibre and Polymer Technology, Division of Wood Chemistry and Pulp Technology, Stockholm, Sweden. 6 pp.

Hon DNS, Shiraishi N (2000) Wood and cellulosic chemistry. CRC Press, Boca Raton, FL. 300-501 pp.

IMA-Europe (2006) Calcium Carbonate, Brussels, Belgium. http://www.ima-eu.org/fileadmin/cca/CalCarb05.pdf. (10 June 2010)

Iwamoto S, Nakagaito AN, Yano H, Nogi M (2005) Optically transparent composites reinforced with plant fiber-based nanofibers. Appl Phys Mater Sci Process 81(6): 1109-1112.

Iwatake A, Nogi M, Yano H (2008) Cellulose nanofiber-reinforced polylactic acid. Compos Sci Tech 68 (9): 2103-2106.

Jonoobi M, Harun J, Shakeri A, Misra M, Oksman K (2009) Chemical composition, crystallinity, and thermal degradation of bleached and unbleached kenaf (*Hibiscus cannabinus*) bast pulp and nanofibers. BioResources 4(2): 626-639.

Joshi SV, Drzal LT, Mohanty AK, Arora S (2004) Are natural fiber composites environmentally superior to glass fiber reinforced composites? Composites: Part A 35(3): 371-376.

Kaldor AF, Karlgren C, Verwest H (1990) Kenaf-a fast growing fiber source for papermaking. Tappi J 73(11): 205-208.

Keshk S, Suwinarti W, Sameshima K (2006) Physicochemical characterization of different treatment sequences on kenaf bast fiber. Carbohydr Polymer 65(2):202-206.

Klemm D, Schmauder HP, Heinze T (2005) Cellulose. Wiley Online Library. Weinheim, Germany. http://www.wiley-vch.de/books/biopoly/pdf_v06/bpol6010_275_287.pdf . (20 May 2011)

Kono H, Numata Y (2004) Two-dimensional spin-exchange solid-state NMR study of the crystal structure of cellulose II. Polymer 45 (13): 4541-4547.

Kovalenko VI (2010) Crystalline cellulose: structure and hydrogen bonds. Russ Chem Rev 79 (3): 231 - 241.

Kuruvilla J, Sabu T, Pavithran C (1996) Effect of chemical treatment on the tensile properties of short sisal fibre-reinforced polyethylene composites. Polymer 37(23): 5139-5149.

Kvien I, Oksman K (2007) Orientation of cellulose nanowhiskers in polyvinyl alcohol. Appl Phys Mater Sci Process 87(4): 641-643.

Lahiji RR, Xu X, Reifenberger R, Raman A, Rudie A, Moon RJ (2010) Atomic force microscopy characterization of cellulose nanocrystals. Langmuir 26 (6): 4480-4488

Lee HJ, Han YS, Yoo HJ, Kim JH, Song KH, Ahn CS (2003) Effect of chemical retting on the fiber separation of kenaf bast. KSCT 27(9-10): 1144-1152.

Lee SY, Mohan DJ, Kang IA, Doh GH, Lee S, Han SH (2009) Nanocellulose reinforced PVA composite films: effects of acid treatment and filler loading. Fibers and Polymers 10(1):77-82.

Lee S, Shi SQ, Barnes MH (2007) Multifunctional nanoparticles at the hydrophilic and hydrophobic interface. Page 173-181 in CY Hse, Z Jiang and ML Kuo, eds Proc Advanced Biomass Science and Technology for Bio-Based Products, 23-25 May 2007, Beijing, China.

Lee S, Shi SQ, Groom LH, Xue Y (2010) Properties of unidirectional kenaf fiber-polyolefin laminates. Polymer Compos 31(6):1067-1074.

Lee S, Shupe TF, Groom LH, Hse CY (2007) Thermomechanical pulp fiber surface modification for enhancing the interfacial adhesion with polypropylene. Wood Fiber Sci 39(3): 424-433.

Leitner J, Hinterstoisser B, Wastyn M, Keckes J, Gindl W (2007) Sugar beet cellulose nanofibril-reinforced composites. Cellulose 14(5):419-425.

Lewin M (2006) Handbook of Fiber Chemistry. CRC Press, Boca Raton, FL. 776 pp.

Li J (2002) Wood Science. China Higher Education Press. Beijing, China. 106-107 pp.

Lloyd EH, Seber D (2006) http://www.hempology.org/Current History/1996 Hemp Composites.html.

Lu J, Wang T, Drzal LT (2008) Preparation and properties of microfibrillated cellulose polyvinyl alcohol composite materials. Composites: Part A 39 (5): 738-746.

Mago G, Kalyon DM, Fisher FT (2009) Polymer crystallization and precipitation-induced wrapping of carbon nanofibers with PBT. J Appl Polymer Sci 114(2): 1312-1319.

Mani P, Satyanarayana KG (1990) Effects of the surface treatments of lignocellulosic fibers on their debonding stress. J Adhes Sci Tech 4(1): 17-24.

Marcovich NE, Auad ML, Bellesi NE, Nutt SR, Aranguren MI (2006) Cellulose micro/nanocrystals reinforced polyurethane. J Mater Res 21(4): 870-881.

Michell A (1986) Composites containing wood pulp fibres. Appita J 39(3): 223-229.

Mohanty A K, Drzal LT, Misra M (2002) Engineered natural fiber reinforced polypropylene composites: influence of surface modifications and novel powder impregnation processing. J Adhes Sci Tech 16(8): 999-1015.

Mohanty A K, Misra M, Hinrichsen G (2000) Biofibres, biodegradable polymers and biocomposites: an overview. Macromol Mater Eng 276-277(1): 1-24.

Mohanty A K, Drzal LT, Misra M (2002) Novel hybrid coupling agent as an adhesion promoter in natural fiber reinforced powder polypropylene composites. J Mater Sci Lett . 21(23):1885-1888.

Mohanty A K, Drzal LT, Misra M (2002) Sustainable bio-composites from renewable resources: opportunities and challenges in the green materials world. J Polymer Environ. 10(1-2):19-26.

Morrison WH, Akin DE, Ramaswamy G, Baldwin B (1996) Evaluating chemically retted kenaf using chemical, histochemical, and microspectrophotometric analyses. Textil Res J 66(10):651–656.

Mwaikambo LY (2006) Review of the history, properties and application of plant fibers. AJST 7(2): 120-133.

Nadkarni VM, Jog JP (1991) Two-phase polymer systems. Hanser Publishing, New York. 213 pp.

Nakagaito AN, Yano H (2005) Novel high-strength biocomposites based on microfibrillated cellulose having nano-order-unit web-like network structure. Appl Phys Mater Sci Process 80(1):155-159.

Nishino T, Takano K, Nakamae K (1995) Elastic modulus of the crystalline regions of cellulose polymorphs. J Polymer Sci Polymer Chem 13(11): 1647-1651.

Nogi M, Ifuku S, Abe K, Handa K, Nakagaito AN, Yano H (2006) Fiber-content dependency of the optical transparency and thermal expansion of bacterial nanofiber reinforced composites. Appl Phys Lett 88(13): 133124-133124-3.

Nogia M, Handa K, Nakagaito AN, Yano H (2005) Optically transparent bionanofiber composites with low sensitivity to refractive index of the polymer matrix. Appl Phys Lett 87(24): 243110-243110-3.

Nugmanov OK, Pertsin AI, Zabelin LV, Marchenko GN (1987) The molecular-crystal structure of cellulose. Russ Chem Rev 56(8):764-776.

Oksman K, Mathew AP, Bondeson D, Kvien I (2006) Manufacturing process of cellulose whiskers/polylactic acid nanocomposites. Compos Sci Tech 66 (15): 2776-2784.
Oliver WC, Pharr GM (1992) An improved technique for determining hardness and elastic modulus using load and displacement sensing indentation experiments. J Mater Res 7(6):114-117.

Othman R, Zakaria S, Chia CH, Zuriyati A, Isa N (2010) Mechanical and optical properties of $CaCO_3$ lumen-loaded paper: effect of polyethylenimine and alum. Sains Malaysiana 39(3): 435-439.

Parikh DV, Calamari TA, Sawhney APS, Blanchard EJ, Screen FJ, Warnock M, Muller DH, Stryjewski DD (2002) Improved chemical retting of kenaf fibers. Textil Res J 72(7) : 618-624.

Pettersen RC (1984) The chemistry of solid wood. Page 76-81 *in* RM Rowell, eds. The chemical composition of wood. American Chemical Society, Washington DC.

Presser V, Gerlach K, Vohrer A, Nickel KG, Dreher WF (2010) Determination of the elastic modulus of highly porous samples by nanoindentation: A case study on sea urchin spines. J Mater Sci 45(9): 2408-2418.

Qua EH, Hornsby PR, Sharma HSS, Lyons G, McCall RD (2009) Preparation and characterization of poly(vinyl alcohol) nanocomposites made from cellulose nanofibers. J Appl Polymer Sci 113(4): 2238-2247.

Ramaswamy GN, Ruff CG, Boyd CR (1994) Effect of bacterial and chemical retting on kenaf fiber quality. Textil Res J 64(5): 305-308.

Roohani M, Habibi Y, Belgacema NM, Ebrahim G, Karimi AN, Dufresne A (2008) Cellulose whiskers reinforced polyvinyl alcohol copolymers nanocomposites. Eur Polymer J 44 (8):2489-2498.

Rowell RM, Jacobson R, Caulfield D (1999) Kenaf properties, processing and products. Page 381-392 *in* Properties of kenaf/polypropylene composites. Ag. & Bio. Engineering, Mississippi State University, Starkville, MS.

Rusli R, Eichhorn SJ (2008) Determination of the stiffness of cellulose nanowhiskers and the fiber-matrix interface in a nanocomposite using raman spectroscopy. Appl Phys Lett 93(3): 033111-033111-3.

Saha BC (2003) Hemicellulose bioconversion. J Ind Microbiol Biotechnol 30(5): 279-291.

Salam A, Reddy N, Yang Y (2007) Bleaching of Kenaf and corn husk fibers. Ind Eng Chem Res 46(5):1452-1458.

Samal RK, Ray MC (1997) Effect of chemical modifications on FTIR spectra II: physicochemical behavior of pineapple leaf fiber (PALF). J Appl Polymer Sci 64(11): 2119-2125.

Sanadi AR, Hunt JF, Caulfield DF, Kovacsvolgyi G, Destree B (2001) High fiber-low matrix composites: kenaf fiber/polypropylene. Pages 121-124 in Proc The Sixth International Conference on Woodfiber-Plastic Composites, 15-16 May, 2001, Madison, WI.

Sarko A, Muggli R (1974) Packing analysis of carbohydrates and polysaccharides III: valonia cellulose and cellulose II. Macromolecules 7(4):486-494.

SAS (2008) SAS Institute Inc. Version 9.2. Cary, NC, USA

Schubnell M (2001) Determination of Polymer Crystallinity with DSC Measurements. UserCom No. 1. 12-13 pp.

Segal L (1959) An empirical method for estimating the degree of crystallinity of native cellulose using the X-ray diffractometer. Textil Res J 29(10): 786-794.

Shi SQ, Lee S, Shi J (2008) Lamination process for chemical retted kenaf fiber/thermoplastic polymer composites *in* Proc 23rd Annual American Society for Composites Technical Conference, 9-11September, Memphis, TN.

Shi SQ, Lee S, Horstemeyer M (2007) Natural fiber retting and inorganic nanoparticle impregnation treatment for natural fiber/polymer composites *in* Proc American Society for Composites, 17-19 September, Seattle, WA.

Shibata S, Cao Y, Fukumoto I (2006) Lightweight laminate composites made from kenaf and polypropylene fibres. Polymer Test 25(2): 142-148.

Siqueira G, Bras J, Dufresne A (2009) Cellulose whiskers versus microfibrils: influence of the nature of the nanoparticle and its surface functionalization on the thermal and mechanical properties of nanocomposites. Biomacromolecules 10(2):425-432.

Song KH, Obendorf SK (2006) Chemical and biological retting of kenaf fibers. Textil Res J 76(10): 751-756.

Sturcova A, Davies GR, Eichhorn SJ (2005) Elastic modulus and stress-transfer properties of tunicate cellulose whiskers. Biomacromolecules 6(2):1055-1061.

Takashi N, Hirao K, Kotera M, Nakamae K, Inagaki H (2003) Kenaf reinforced biodegradable composite. Compos Sci Tech 63(9): 1281-1286.

Tang C, Liu H (2008) Cellulose nanofiber reinforced poly(vinyl alcohol) composite film with high visible light transmittance. Compos Appl Sci Manu 39 (10):1638-1643.
TAPPI (1993) T 211 om-93. Ash in wood, pulp, paper and paperboard: combustion at 525 degrees celsius. Englewood, CO.

The Institute of Paper Chemistry (1951) Method No. 482. Appleton, Wisconsin.

Tsuchida T, Yoshinaga (1997) Production of bacterial cellulose by agitation culture systems. Pure Appl Chem 69(11):2453-2458.

Updegraff DM (1969) Semimicro Determination of Cellulose in Biological Materials. Anal Biochem 32(3): 420-424.

Wambua P, Ivens J, Verpoest I (2003) Natural fibres: can they replace glass fibre reinforced plastics? Compos Sci Tech 63 (9): 1259-1264.

Wang G, Yu Y, Shi SQ, Wang J, Cao S, Cheng H (2011) A micro-tension test method for measuring tensile properties of individual cellulosic fibers. Wood Fiber Sci, in press.

Wang J, Ramaswamy G (2003) One-step processing and bleaching of mechanically separated kenaf fibers: effects on physical and chemical properties. Textil Res J 73 (4): 339.

Wang S, Cheng Q, Rials TG, Lee SH (2006) Cellulose microfibril/nanofibril and its nanocompsites. Page 301-308 *in* MNM Yusoff, eds Proc The 8th Pacific Rim Bio-based Composites Symposium, 20-23 November, 2006, Kuala Lumpur, Malaysia.

Wise LE, Murphy M, Addieco AD (1946) Chlorite holocellulose, its fractionation and bearing on summative wood analysis and on studies on the hemicelluloses. Paper Trade J 122(2): 35-43.

Woodcock C, Sarko A (1980) Packing analysis of carbohydrates and polysaccharides 11: Mmolecular and crystal structure of native ramie cellulose. Macromolecules 13(5):1183-1187.

Wu Q, Henriksson M, Liu X, Berglund LA (2007) A high strength nanocomposite based on microcrystalline cellulose and polyurethane. Biomacromolecules 8 (12): 3687-3692.

Xiang Q, Lee YY, Pettersson PO, Torget RW (2003) Heterogeneous aspects of acid hydrolysis of α-cellulose. Appl Biochem Biotechnol 107(1-3): 505-514.

Zadorecki PJ, Michell AJ (1989) Future prospects for wood cellulose as reinforcement in organic polymer composites. Polymer Compos 10(2): 69-77.

Zampaloni M, Pourboghrat F, Yankovich SA, Rodgers BN, Moore J, Drzal LT, Mohanty AK, Misra M (2007) Kenaf natural fiber reinforced polypropylene composites: a discussion on manufacturing problems and solutions. Composites: Part A 38(6): 1569-1580.